MEASURING STRAINS DURING CONSTRUCTION OF A STEEL BUILDING USING A WIRELESS SENSOR NETWORK

by

Tayler Christine Wennick

A thesis submitted to the Faculty of the University of Delaware in partial fulfillment of the requirements for the degree of Master of Civil Engineering

Summer 2016

MEASURING STRAINS DURING

CONSTRUCTION USING A

WIRELESS SENSOR NETWORK

by

Tayler Christine Wennick

Approved: _____

Thomas Schumacher, Ph.D.
Professor in charge of thesis on behalf of the Advisory Committee

Approved: _____

Harry W. Shenton III, Ph.D.
Chair of the Department of Civil & Environmental Engineering

Approved: _____

Babatunde A. Ogunnaike, Ph.D.
Dean of the College of Engineering

Approved: _____

Ann L. Ardis, Ph.D.
Senior Vice Provost for Graduate and Professional Education

ACKNOWLEDGMENTS

I would like to thank all people who contributed in some way to the work described in this thesis. Specifically, I would like to personally thank my advisor Dr. Thomas Schumacher for his support and patience throughout this project. Throughout my engineering career, his kindness and enthusiasm played a great part in shaping my academic future. I would not be where I am today if it was not for his support, generosity, and guidance.

Thank you to the University of Delaware and the many people I've met here. My undergraduate and graduate experience benefitted greatly from the courses I took and the professors that taught them. I would like to thank Philipp Keller, Dr. Jennifer McConnell, and Gary Wenczel for their various forms of support during my graduate study.

Most importantly, none of this would have been possible without the love and support from my family. I would like to express my heartfelt gratitude for their encouragement and strength throughout this endeavor. You helped me through the rough days and late nights with words of encouragement and love. These words fail to express the amount of thankfulness and love I have for you all. Without my family, this adventure would have never been possible.

Finally, I offer my regards and blessings to all of those who supported me in any respect during the completion of my thesis.

TABLE OF CONTENTS

LIST OF TABLES

LIST OF FIGURES

ABSTRACT

Nationwide, there is a well-known need for sustainable structural engineering practices in order to reduce the carbon footprint associated with manufacturing and constructing steel members. While the reuse of structural steel would significantly decrease the environmental impacts associated with civil construction, this practice is rare. Uncertainties regarding the structural integrity of reused steel members are the cause of such minimal steel reuse implementation. To address these concerns, the full strain history of a steel member from its arrival at the construction site through significant portions of its service life is recorded. In this thesis, a full test, analysis, and review is conducted on the components of a wireless sensing network used for wirelessly instrumenting an addition to Purnell Hall on the University of Delaware campus. The use of a wireless sensing network and a wireless instrumentation plan is motivated by the basis that the greatest concerns regarding future structural integrity in a reuse application are during construction and in the vicinity of connections.

Chapter 1

INTRODUCTION

1.1 Project Description

Buildings are what create the indoors. Evolving from the cave, to wooden huts, to brick houses, to drawbridge castles and finally staggering skyscrapers, the building has been fundamental in human society. However, whether the building is a one-floor house or a one hundred story skyscraper, it is not meant to last forever. The world's environment is degrading and the amount of natural resources is limited. Structural engineers now face a new set of parameters in order to improve the sustainability of civil infrastructure and reduce the environmental footprint of the construction industry. This thesis research was supported by the NSF-funded research project entitled "Reuse of Structural Steel: Towards Maximizing the Greenness of Buildings" (Award # 1336478). The intended outcome of the project is to cultivate a cultural shift in the way buildings are designed, constructed, deconstructed, and repurposed.

Buildings are not meant to last forever. Structural engineers design buildings based on a service life, in which a building is designed to fulfill its intended purpose for a given number of years after construction, commonly 50 years today (Sarja 2002). At the end of a building's life, the building and all of its structural elements enter the end-of-life stage. There are three possible choices for the end-of-life stage. The first choice is that the building is demolished and the materials are sent to a landfill. 40% of the world's materials flow from extraction to landfill for new construction,

maintenance, renovation, and demolition of buildings (Webster and Costello 2005). This statistic brews environmental concerns since disposing steel in a landfill is the least sustainable option. In 2012, the U.S. industrial process-related emissions for iron and steel production totaled 53.8 Tg CO_{2e}, which is 37.2% of the U.S. CO_{2e} emissions from all industrial processes (EPA 4-3 2013). The second option is recycling. Steel, which is a major structural component of buildings, is a highly recycled material because it is 100% recyclable without impairment to its physical properties such as strength, density, durability, ductility, and corrosion resistance (World Steel Association 2013). However, there are still detrimental impacts to the environment when recycling steel. An electric arc furnace manufacturing process (EAF) is utilized to accomplish steel recycling. Through the EAF process, an average of 0.875 tons of CO_{2e} per ton of structural steel is produced (Weisenberger 2010). Further, the energy intensity of EAF for primary steel construction consumes 28.3-30.9 GJ/ton and for secondary steel production consumes 9.1 – 12.5 GJ/ton of crude steel (Yellishetty, et al. 2011). According to AISC, the production of hot-rolled structural shapes in the U.S. in 2013 exceeded 6.5 million tons (AISC 2015). According to these numbers, in 2013, the best case scenario was that 5.5 million tons of CO_{2e} emissions were produced and 60 million GJ of energy was consumed in one year. Therefore, the end-of-life stage for structural steel can still be improved. The third and most sustainable end-of-life solution is reuse. Reusing steel members eliminates the environmental impacts that recycling plants pose, such as CO_2 emissions and energy consumption. Energy input required in reusing a steel member includes the energy needed to modify members, i.e. cut off sections of concern or removing unwanted sections, and the energy involved in the transportation of a member to a new site (Silverstein 2009).

Therefore, the greenest end-of-life option is reusing structural steel members. Today, 87% of the world's heavy structural steel is recycled, 11% is reused, and 2% is taken to a landfill (Durmisevic and Noort 2003). In order to improve the impact buildings have, reusing structural steel components is the environmentally preferred alternative.

The reduce – reuse – recycle mantra can be utilized for structural steel in buildings. First, reduce or minimize material consumption. Then, reuse the material as many times as possible. Finally at the end of a steel member's service life, the material is recycled. However, this is far from the current practice in the United States. The United States recycles 98% of steel used in construction (Yellishetty, et al. 2011). According to a survey conducted by Gorgolewski et al. (2006) in order to understand the opportunities and concerns related to structural steel reuse, the largest concern with using reclaimed steel components for new construction in Canada was the reliability and safety of second-hand materials and the liability in the event of their failure. This is assumed to be synonymous to U.S. construction and engineering practices. Many steel service centers feel as though engineers will not support the use of materials with unknown characteristics and load histories (Gorgoleweski, et al. 2006).

The overall objective of the NSF research project is to prove the hypothesis that widespread reuse of structural steel for buildings is structurally-sound engineering practice with significant environmental benefits through simulation, analysis, laboratory experimentation, and field measurements. This objective can be accomplished based on evaluating the hypothesis that primary and secondary structural steel members in buildings can be safely reused without recycling. Due to the fact that up to a high yield stress steel behaves linear-elastically and further due to

safety factors present in the steel member's design, a steel member can be loaded repeatedly with its design loads without any compromise in performance. Further, it can also be accomplished based on evaluating the hypothesis that construction-induced and localized stresses near connections may cause stresses that can be reliably predicted with the use of advanced simulation techniques such as finite element modeling (FEM) for assurance purposes in future reuse applications. The hope of the proposed research outcome is that a cultural shift in the way materials are regarded in the engineering society and profession will occur toward reuse of structural steel.

1.2 Thesis Objective

The ultimate objective of this thesis is to successfully implement a wireless sensor network (WSN) during construction in order to capture peak strains of a building during construction and selected periods of its service life.

Before a WSN can be utilized in the field, one must first implement and verify a proposed structural health monitoring (SHM) system on a full-scale laboratory specimen. Through experimental instrumentation in the University of Delaware (UD) Structures Laboratory before field instrumentation, the system was tested, debugged, and programmed in a controlled and repeatable environment. This is to ensure that opportunities for capturing unique data during the actual construction stage are maximized. The data collected from the WSN can then be utilized to determine the history of construction-induced stresses. During the construction of a building, situations where the actual stresses a steel member experiences are predicted less confidently include when field conditions, fit up problems, and temporary loadings may differ from the designer's expectations, and in the vicinity of connections. The peak strains collected using the WSN can then provide information regarding the

construction forces the building's steel members experience. The verification of the WSN and the data collected from the instrumentation of the building will provide the foundation for determining less known construction and connection stresses of a steel member.

1.3 Literature Review

1.3.1 Reuse of Steel Members

Due to the environmental benefits that the reuse of structural steel presents, designers are starting to incorporate reused steel members into construction projects. This is because of the greater environmental benefits that result from reusing steel components rather than recycling them. Further, reusing structural members can gain credits in LEED certification. According to Fujita and Iwata (2008), the recycling of iron and steel materials is now at a turning point due to the time-consuming scrapping process and management problems that exist at the electric furnace manufacturers. Therefore, there has been a rise in the need for implementation of reusing structural steel. Steel is the only type of structural member that can be reprocessed. Again, since reusing structural members only requires ancillary energy for demolition, transportation, and adjustments, it is preferable over the recycling process which requires substantial energy consumption and CO_2 emissions. Steel undergoes no major changes throughout its lifetime other than corrosion and local plastification caused by unusually high loads. Corrosion problems are solved by painting. Plastification caused by extreme events, such as earthquakes, can be handled by

adopting damage-controlled design. A damage-controlled structure is defined as "a combination of several structural systems and energy transformation devices that are integrated in such a way as to restrict damage to a specific set of structural elements that can be readily repaired" (Connor, et al. 1997). Thus, reusing structural steel for construction projects is a reliable practice that can lead to sustainable structures. (Fujita and Iwata 2008)

Skepticism towards structural steel reuse and the traditions of the construction industry are standing in the way of reuse becoming the next step towards a more sustainable construction industry. According to Gorgolewski (2006), reuse of steel components requires designers and contractors to be more flexible and creative since salvaged components may not be readily available off the shelf and may be difficult to source. Therefore, one of the principal problems with reuse is coordinating demand with supply. If designing a structure with reused components, salvaged steel of the required size may not be readily available. Designers can either redesign the structure to suit the available salvaged components or opt for an oversized component that is available. However, to maximize the potential for reuse even further, Gorgolewski (2006) suggests that the starting point for a new design in the future will be based on an inventory of available materials from salvage. Other problems outlined in a survey of the steel construction industry by Gorgolewski et al. (2006) included liability, traceability, unknown specifications, and cost of deconstruction to name a few. Designing a structure for disassembly, which is described in more detail in section 5.2, is an addition way to address these obstacles. Currently, the challenges posed by integrating salvaged steel components into new buildings discourage designers,

contractors, and clients from embracing structural steel reuse. (Gorgolewski, "Implications of Reuse and Recycling" 2006)

1.3.2 Structural Health Monitoring of Buildings

In order to address the concerns in the engineering and construction sector with regards to the liability of the structural integrity of reused steel components for buildings, structural health monitoring (SHM) techniques can be employed. The objectives of SHM are to measure and characterize the response of the structure due to its experienced loads. According to Rainieri and Fabbrocino (2010), the goal of SHM for civil structures is not only detection of abrupt damages due to extreme events but also monitoring progressive damage or structural performance under operational conditions. Its potential for economic, environmental, and life-safety benefits defines its importance in the civil engineering field. For this research, utilizing a SHM system on a building during construction will provide the necessary measurements to characterize the currently ambiguous structural behavior of steel members during the erection process.

Farrar and Worden (2007) provide an introduction to SHM. According to this article, the civil engineering community has studied vibration-based damage assessment of bridges and buildings since the 1980s. The primary features used to identify damage in these structures are modal properties which can be derived into mode shape curvature and dynamic flexibility (Farrar and Worden 2007). However, the application of SHM to building structures is not as widespread as its application to bridge structures (Ni, et al. 2009). Of the few SHM applications on buildings that can be found, most employ a global monitoring strategy in which strain and acceleration measurements are used to determine global damage of the structure (Cho, et al. 2008).

This research is utilizing a SHM system for localized information of data from steel members during construction, which is seemingly non-existent, but important to quantify in order to determine the strains a member experiences near connection details and other locations of concern.

Although localized SHM for steel buildings during construction has never been performed, there have been a few examples of global SHM of buildings during construction. Some examples include the Titanium La Portada Building (Nunez, Boroschek, and Larrain 2011), the Dongsheng Garden A5 Building (Li, et al. 2012), and the Guangzhou New TV Tower (Ni, et al. 2009).

In order to validate a construction process, Nunez, Boroschek, and Larrain (2011) installed a SHM network during the construction of the Titanium La Portada Building. The Titanium La Portada building stands 56 stories above the ground with 7 underground stories and is a frame-wall concrete building. The construction process lasted from January 2007 to December 2009. During the construction process, the SHM network recorded the vibrations produced by ambient, construction, and earthquake excitations which were then used to identify the natural periods, mode shapes, and damping ratios of the structure. Accelerometers were used for the continuous monitoring system. This information was then compared at different states of the construction using finite element (FE) models that predicted the dynamic response of the structure. For the first three modes, the differences between the measured and predicted natural periods were less than 15%. The reasonable agreement between the model and the experimentally determined mode shapes validated the construction process and permitted the structural engineer to confirm predictive models, anticipate possible abnormal behavior during the construction

process, and take proper actions before the construction process advanced to the next stage. Difficulties related to the non-stationary vibrations caused by impact, the operation of machinery, and the continuous variations in mass and stiffness emerged during the ambient vibration monitoring in a construction environment. These construction operations generated local effects on the structure, which are not representative of the structure's dynamic behavior and were thus ignored. The continuous monitoring of the dynamic properties of the Titanium La Portada building is an excellent example of quality assurance in construction. (Nunez, Boroschek, and Larrain 2011)

In an investigation performed by Li, et al. (2012), a monitoring system consisting of Fiber Bragg grating (FBG) sensors was designed to monitor temperature increase within concrete due to the hydration process, strain variation of the main column on the underground floor relative to subsequent additions of upper floors, and relative long-term displacement between two sinking foundation blocks on the Dongsheng Garden A5 building. The building is an 18-story frame-shear wall residential building and includes one underground floor for parking. FBG temperature and strain sensors were bonded on the rebars of the column and the first floor beam before concrete pouring and then operated continuously for five months afterwards. For this investigation, the measured temperatures agree well with the recorded temperatures. Strain variation of concrete follows the temperature variation trend, which indicates that the strain measured in concrete was mainly attributed to the thermal expansion and contraction of concrete, but not to external forces. Further, the build-up of compressive strains is caused by the addition of multiple floors. Anomalies in strain measurements are postulated to be due to workers unevenly laying

construction material on the column, thus subjecting the rebar to unequal loads. Through this SHM investigation, a thorough understanding of loading variations of the main column of the underground floor during construction of a building could be established. (Li, et al. 2012)

The Guangzhou New TV Tower (GNTVT) located in Guangzhou, China, is a supertall tube-in-tube structure rising to 2000 ft (610 m). Ni, et al. (2009), along with The Hong Kong Polytechnic University implemented a sophisticated long-term SHM system consisting of more than 600 sensors on the building and based on the modular design concept to monitor it during both construction and in-service stages. The motivation behind such an integrated monitoring system lies in being able to track complete data histories from the onset of construction and enabling life-cycle monitoring and assessment of the structure from its birth. Ni, et al. (2009), describe key technological issues in developing and implementing the SHM system throughout the paper. Appropriate selection and placement of sensors is paramount in order to detect the structural damage reliably. Sixteen different types of sensors were employed, which can be broken down into the three categories of parameters of load sources, structural responses, and environmental effects. Sensors were selected based on their ability to capture all important information about the structural static and dynamic properties, to combine multiple types of sensors for accurate measurement of a certain structural response, and various types of sensors should be collocated at crucial locations for cross-calibration. Critical cross-section locations, which are locations suffering large stresses under construction, were determined through finite element analysis on the structure at critical construction stages. Installation of surface mounted sensors occurred either during the construction stage due to the

inaccessibility when scaffolds are dismantled or welded at the workshop. The monitoring system on the GNTVT reports cumulative strain rather than monitoring dynamic strain, which is what a majority of existent SHM collect. Cumulative strain is necessary for evaluating the real safety index of structural components and the impact of extreme events on the structural performance. For synchronous acquisition of strain and temperature data, a wireless system transmits real-time data from the sub-stations to the site office during construction. The wireless system can transmit the data at a speed of 100 Mbps with a maximum transmission distance of 1.25 miles (2 km). For acceleration and other vibration based measurements, wired cabling networks are used. Ni, et al. (2009), concluded that it is difficult to identify the local structural damage for large-scale structures by using modal properties only. Further, it was stated that "a more reliable structural health evaluation is based on multilevel data fusion through combing the global modal properties and the local strain information." Therefore, the GNTVT enabled embedded and surface mounted sensors to monitor in-construction and in-service stresses from the structure's birth. (Ni, et al. 2009)

1.3.3 Wireless Sensor Networks

Wireless sensor networks (WSNs) are becoming substitutes for traditional tethered SHM systems. WSNs consist of the following main components: input sensors, wireless nodes, gateways, and a user interface software, which can be seen in Figure 1. Input sensors are measurement gauges wired to a wireless node that measures response entities such as acceleration, strain, displacement, and more. The wireless node enables simultaneous, high-speed sensing from multiple input sensors to the gateway without the need to install or maintain wires. The wireless gateway coordinates and schedules communication between the remote wireless sensor nodes.

By allowing users to easily control data acquisition preferences, the software platforms streamline network configuration. (LORD MicroStrain)

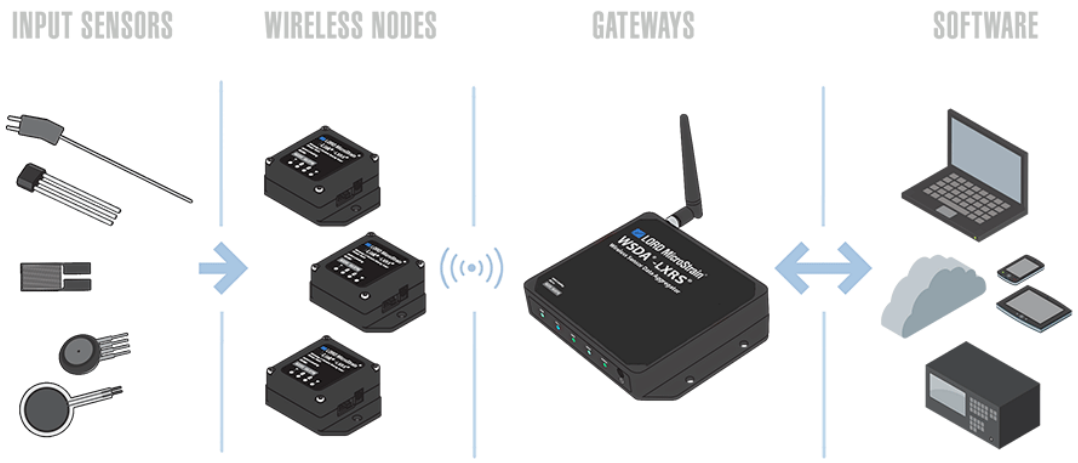

Figure 1: Individual components of a WSN (LORD MicroStrain)

A comprehensive summary of the collective experience that the structural engineering community has gained from the use of wireless sensing for monitoring structural performance and health is presented by Lynch and Loh (2006). Traditional SHM systems employ cabling for communication between sensors and the repository which provides a very reliable communication link but with high financial and labor costs. Therefore, most SHM systems utilizing tethered networks are expensive to install and have low nodal densities. To address these limitations, WSNs were chosen for their low installation costs and greater nodal densities permitted. Further, with a large number of sensors installed on a single structure, wireless monitoring is better suited to implement local-based damage detection. Advantages of using a commercial WSN platform for academic research teams include immediate out-of-the-box

operation, available technical support from manufacturers, and low unit costs. Some advanced systems allow for the collocation of computational power with the sensing transducer transforms the wireless monitoring system into a holistic SHM methodology where damage detection and reporting is fully automated. Lynch and Loh (2006) further point out that WSNs are still in their infancy. Their limitations include the finite energy sources to power devices in the field and thus necessitate alternative power sources. Additional research suggested to test WSNs in longer-term deployment could offer opportunities to refine duty cycle usage strategies, to assess system performance versus environmental factors, and to test the long-term reliability of WSNs. (Lynch and Loh 2006).

WSNs have been implemented in bridges more so than buildings. Nordblom and Galbreath (2012) analyze the applications that LORD MicroStrain's wireless sensor network can accomplish for long-term bridge SHM. Sensing capabilities include vibration, load, strain, displacement, temperature, corrosion, and tilt/inclination, and virtually any sensor can be used with the MicroStrain network. In order to address the wireless networks limitation on energy usage, MicroStrain offers efficiently scheduled data transmission protocols as well as an event driven sleep mode to maintain requisite data with minimal power. The Ben Franklin Bridge that connects Philadelphia, PA to Camden, NJ, the Great Road State Bridge in North Smithfield, RI, the Goldstar Bridge spanning the Thames River in New Haven, CT, and the Corinth Canal Bridge in Corinth, Greece have all employed MicroStrain's WSNs. The MicroStrain WSN makes bridge monitoring systems less disruptive to install and easier to manage. (Nordblom and Galbreath 2012)

WSNs have also been used on bridges during construction. Chacón, et al. (2009) attempted to validate a WSN for strain monitoring during a steel bridge launching by taking strain measurements with conventional pre-wired gauges as well as with newly developed wirelessly connected strain-measuring system. Strain gauges were bonded in zones of the flanges and web where high stresses were expected to occur on a bridge during the construction phase. The gauges measured strain as a function of their resistance variance so that the state of strain at a point of a material and its direction is known. The results showed that pre-wired readings versus wireless readings versus the ABAQUS model readings were all relatively similar. Therefore, Chacón, et al. (2009) were able to validate the wireless system and prove its reliability.

WSNs are also utilized in buildings; however, these SHM systems only globally monitor the building for the development of vibrational mode shapes and they are rarely utilized during construction. One such example is the SHM of historical heritage buildings in Sicily, Italy. Anastasi, Lo Re, and Ortolani (2009) used a WSN to study the dynamics of a site in order to monitor the restoration work carried out on a historical building as a consequence of the damages suffered after a light earthquake. Specifically, they were interested in the response of the structure to vibrations; hence accelerometers were used to collect data in order to better predict the behavior of the structure in reaction to unforeseen loads. This paper outlined Anastasi, Lo Re, and Ortolani's (2009) experience with the setup and design of the WSN on a baroque church. Additional experiments and data collection are still being carried out on the building. (Anastasi, Lo Re, and Ortolani 2009)

Few experiments have investigated the use of WSNs for long-term monitoring of buildings; and if they did, then the experiment only analyzed vibration data. Hoult,

et al. (2010) realized the need to investigate the potential of WSNs for long-term SHM, especially using sensors other than accelerometers. Hoult, et al. (2010) deployed WSNs on several different types of infrastructure systems in London, UK. Again, the advantages of eliminating the cable for SHM of an infrastructure are listed, which include lower system cost, installation time, and system connectivity. To conclude, Hoult, et al. support the use of WSNs due to the offered benefits provided in order for infrastructure managers to have access to better data to support decision making. (Hoult, et al. 2010)

1.3.4 Design for Disassembly

A strategy to lead the industry to reusing rather than recycling structural steel is Design for Disassembly, also known as Design for Deconstruction. Design for Disassembly refers to the concept of planning projects in such a way as to facilitate future renovation and demolition (Catalli and Williams 2001). Using this strategy, a building will become more efficient and adaptable, while also reducing its impact on the environment during demolition. It will revolutionize how a building is designed, maintained, and demolished.

There are many principles originating at the design stage of Designing for Disassembly that will improve the efficiency and economic benefits of deconstruction. Webster and Costello (2005) outlined various guidelines for designing new structures for deconstruction. In regards to the architectural characteristics of a building, two principles to follow are to layer the building systems and to use a simple, regular layout with similar bay sizes throughout. Layering the building systems eases disassembly because intermingling mechanical systems and components makes it difficult to replace these systems during the building's life and to extract the structural

element at the end of its life. Using regular layouts with similar sizes means that the building will yield identical members which are easier to sort, sell, and reuse (Webster and Costello 2005).

There are also structural characteristics engineers can focus on which help in the deconstruction of a building. One of the most important strategies is to develop a deconstruction plan for the building. Such a plan would include a list of building elements with their design life and potential for reuse, as well as instructions for taking the building apart (Silverstein 2009). Further, use common, standard shapes and connections. This will also help in the sorting and selling of identical members. Avoid using composite systems because an extra challenge is posed due to the chance of damaging members while separating them. Use salvaged material in the building since if these members were salvaged once, they can usually be salvaged again. Additional practices structural engineers can use include avoiding multiple types of structural systems, using fewer large members rather than many small members in design, and selecting materials with reuse potential based on current standards. By following these general guidelines, structural engineers can design for disassembly for buildings. (Webster and Costello 2005)

The type of fasteners and connections used is a large component of disassembly. The two most popular types of steel connections are welds or bolts. Welds can be a variety of thicknesses and configurations and thus usually display sudden failure. This is an issue during disassembly because when welds are being deconstructed they can break without warning. Further, removing connections with critical welds necessitates continuous help from a crane to ease the load on the connections. Thus, bolts are the preferable fastener type. Bolts have a usual failure

mode and exhibit plastic deformation prior to failure. When disassembling steel members with bolt holes, members are not strictly reused but rather remanufactured in order to patch the original holes. For structural simplicity and financial concerns, switching between welded and bolted connections on the same project should be avoided (Silverstein 2009).

In order to further facilitate building disassembly, there have been two innovations in connection design. Creating a standardized system in which steel members and connections are chosen from minimal kit parts instead of vast offering of fabricators increases ease of disassembly with large reuse potential. Bolt holes are pre-drilled at the ends of beams and at regular intervals along a column and connection angles and plates are designed to fit the members via an interlocking system. Advantages of a standardized system include quick construction time, improved construction safety and quality, and easy deconstruction. Another innovation is friction connections, synonymous to clamping a wood block on a table surface. Specific friction connection designers are still being created. The main advantage of friction connections over bolted connections is that they do not penetrate the element (Silverstein 2009).

The construction industry can prepare buildings for disassembly by addressing various types of design issues. Builders should consider the handling and safety of members during deconstruction. By planning ahead and providing aid for dismantling members then a deconstruction project can be accomplished quickly and safely. Seek alternatives to spray-on fire-proofing since it is difficult to remove from steel framing and can add shipping weight and volume on salvaged members. Label the materials used in the building on the members. Examples to label include the material grade

and strength, specific handling instructions, date cast, and more. Finally, safeguard original drawings so that they can be easily referenced for future deconstruction. Designing for disassembly of a new structure starts in the design stage, and to ease future deconstruction, one must plan ahead and follow these general guidelines. (Webster and Costello 2005)

Designing buildings for deconstruction or designing buildings with reclaimed components adds a whole new level of complexity to the project. Obstacles in designing for disassembly include worker safety and health hazards, site storage for recovered materials, and lack of standards for certain recovered materials (Pulaski, et al. 2003). Once a building is disassembled, the building components are available to be utilized for new construction. Reusing components reclaimed from demolition requires the designers to be more flexible and willing to adapt their normal processes since reclaimed components are often not readily available from stock and their specifications may not be clear (Gorgolewski, "Designing with Reused Building Components" 2008). Since standard engineering practice is focused on the fastest, easiest, and cheapest way to finish a job, it is imperative to standardize the time, financial, and environmental benefits reusing major structural components will provide so that designers can factor the efforts versus savings into a design. Since reused components do not generally come straight from the shelf and the required size or type of component may not be readily available, "this may necessitate a redesign to suit the available reclaimed components or choosing whichever oversized components are readily available" (Gorgolewski, "Designing with Reused Building Components" 2008). To overcome this obstacle, the starting point of a new design could come from an inventory of available disassembled materials. Thus, the design team for a newly

constructed building will need to do additional research at the start of a project to categorize, find, examine, and decide on appropriate components which could lead to additional cost in design and testing fees (Gorgolewski, "Designing with Reused Building Components" 2008). However, all additional costs can be financially offset by reduced material costs of reclaimed members and environmentally offset by reusing members.

When the architecture, engineering, and construction industry can overcome tradition and skepticism, integrating designing for disassembly into all future new construction will prove to be an economic venture and environmental benefit. The ultimate goal of designing for disassembly is to facilitate a zero-waste and closed-loop material flow system for the built environment. Thus, in order to accomplish this goal, designing buildings for versatility, durability, and simplicity will be designing buildings to reusability. To conclude, designers need to realize that their influence on a structure can extend far beyond the opening ceremony of a new building and into its end-of-life stage by designing for disassembly.

Chapter 2

LABORATORY EVALUATION OF WIRELESS SENSOR NETWORK

2.1 Wireless Sensor Network Selection

A commercial wireless sensor network (WSN) was selected to be used in this research for its ability to record, process, and transmit strain gauge and accelerometer readings wirelessly through its nodes during the construction of a building. The wireless capability is crucial for recording the stress history of steel members from the time they are delivered to the construction site, unloaded, put in place, and to when they are installed into service. Since no wires are present, typical construction practices are followed thus recording a full and accurate stress history without any bias towards instrumented members. Therefore, real, common construction scenarios are represented by the data collected. However, before field instrumentation can take place, laboratory evaluation of the wireless sensor network occurred where the system was tested, debugged, and optimally programmed in a controlled and repeatable environment. This way, opportunities for capturing unique data during the monitoring of a building in construction was maximized.

The WSN employed in this research is manufactured by Lord Microstrain. Lord Microstrain's V-Link –LXRS analog input sensor nodes were chosen for their high-speed sensing and data acquisition from multiple wireless strain gauges and Lord Microstrain's G-Link –LXRS wireless accelerometer node was chosen for acceleration readings. The V-Link –LXRS nodes have four differential and three single-ended analog input channels combined to make seven versatile channels. These nodes can

record up to four wired strain gauge inputs, which are then transmitted wirelessly to the gateway unit. Sample rates up to 10 kHz are possible. Various sampling rates and settings for data-logging are available depending on the desired recording patterns, including continuous, burst, and event-triggered modes. Each node is encased in a waterproof enclosure, which protects the V-Link –LXRS from the elements. The battery in the node has 650 mAh capacity, and the enclosure has two additional D sized batteries with 18,000 mAh capacity each. The G-Link –LXRS includes a triaxial accelerometer with sample rates up to 4096 Hz and with similar sampling and datalogging types as the V-Link –LXRS. Both nodes include an internal temperature sensor for local temperature recordings. (LORD MicroStrain 2015)

In order to coordinate and maintain wireless transmissions across a network of distributed wireless nodes, the gateway is the hub of communication for Lord Microstrain's WSN. The LXRS wireless communication protocol enables high-speed sampling, node synchronization, and transmission with a range up to 2 km (1.24 miles) between nodes and gateways. The gateway is attached to a computer or laptop equipped with the Node Commander software via a USB cable. The Node Commander software allows users to easily program all nodes on a single gateway. Settings users can easily control include sampling rates, data acquisition preferences, and deployment of custom alerting, reporting, and analytics. Lord Microstrain's WSN needed to be studied and validated in the University of Delaware's Structures Laboratory before being used in the field. (LORD MicroStrain 2015)

2.2 Evaluation Setup and Instrumentation

Three wireless nodes were utilized in the current laboratory evaluation. Two V-Link –LXRS nodes were used to record data from a total of eight strain gauges, and

one G-Link –LXRS node recorded triaxial acceleration with its integrated triaxial accelerometer. These instruments were mounted along a 12.5 ft (3.8 m) long W14x87 (W350x129) steel beam, as seen in Figure 2. The strain gauges were produced by Vishay Precision Group and were installed using M-Bond 200 adhesive. The accelerometer node was fixed to the web of the beam with screws. Of the eight strain gauges, five were uniaxial strain gauges and three were dedicated to a strain rosette. Uniaxial strain gauges measure strain in one direction. For this experiment they were oriented to measure longitudinal strain on the beam. One strain rosette was installed, which measures strain in three different orientations, i.e. 0, 45, and 90°, thus requiring three strain gauges. Stress at each gauge location could be calculated from each gauge's measured strain. The strain rosettes could be used to calculate principal strains and stresses using Mohr's circle. The enclosed wireless nodes for the strain gauges were secured to the beam using Velcro.

The locations of the instrumentation can be seen in Figure 3 with the numbered locations referring to strain gauge locations. The unhatched areas represent the region of the beam that are theoretically undisturbed by the applied point loads and support reactions. The disturbed regions were approximated to extend a distance equal to the section depth of the beam from the location of the supports or applied point loads. Strain gauges 3 through 8 are situated in the undisturbed region, i.e. where beam bending theory applies, so that a strain profile for the beam can be created and compared to theoretical values.

Figure 2: Laboratory evaluation setup in the University of Delaware Structures Laboratory

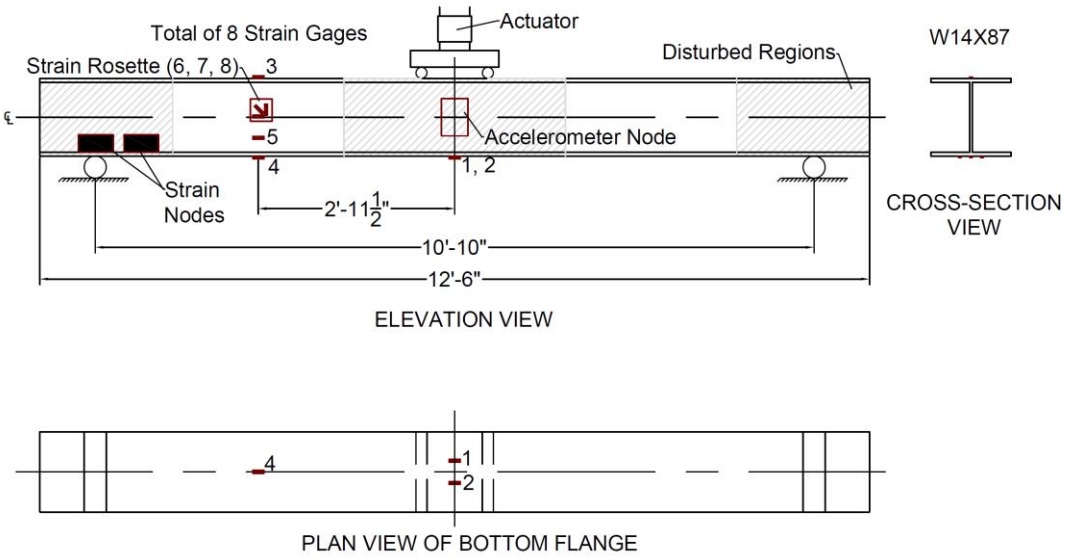

Figure 3: Strain gauge instrumentation of laboratory specimen (Mcconnell, et al. 2014)

2.3 Loading Protocol

Three load tests were applied to the instrumented beam. In the first test, the load was gradually increased to 5 kips (22.25 kN), held constant, and then unloaded. This pattern was repeated with the peak load being 5 kips (22.25 kN) greater than the previous one until a total load of 30 kips (133.5 kN) is reached. The pattern is depicted in Figure 4. 30 kips (133.5 kN) is theoretically equal to 50% of the yield load assuming a yield strength of 36 ksi (250 MPa) and a modulus of elasticity of 29,000 ksi (200,000 MPa).

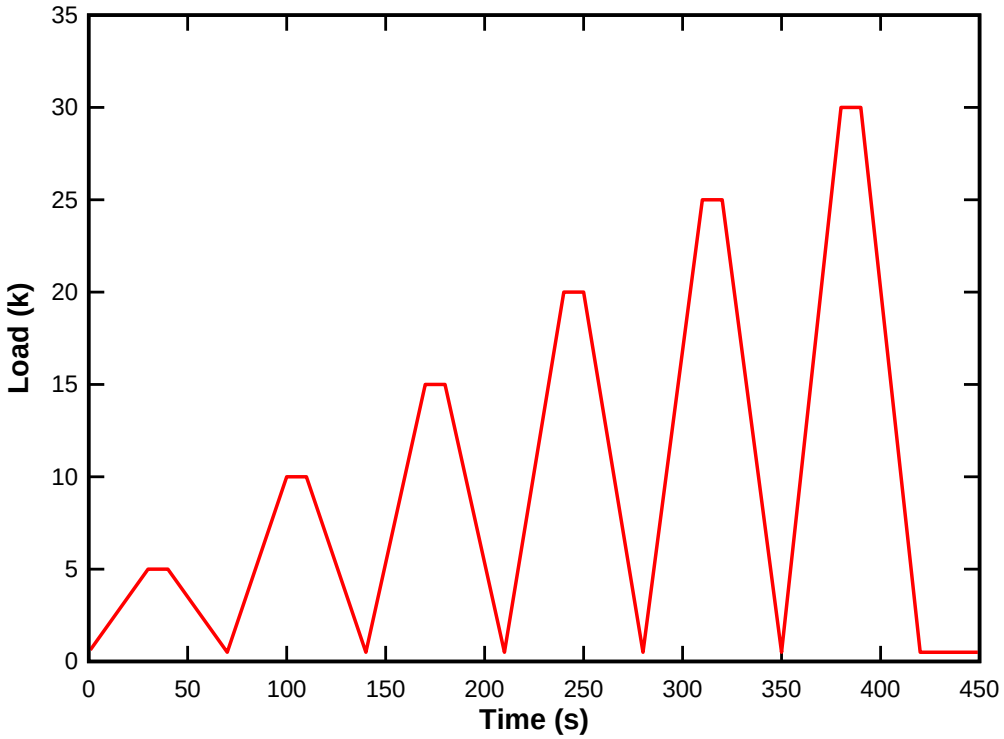

Figure 4: Load induction for scenario 1

The remaining two load tests were of dynamic-type and used to assess the performance of the accelerometer. In the second loading scenario, the beam was loaded to 7.5 kips (33.36 kN) within 10 seconds, and then cycled between 0.5 kips (2.25 kN) and 15 kips (66.75 kN) for various frequencies of 0.5 Hz, 1 Hz, and 2 Hz. The third load test consisted of an impact test in which a hammer was struck one time to the top flange of the beam. From these two tests, the recorded signals were analyzed both in the time and frequency domain.

2.4 Evaluation Results

2.4.1 Load Test 1

Once all data was collected for the first loading scenario, analyzing the data in order to validate the WSN ensued. The first step was comparing the measured with the theoretical strains for loading values 0 kips (0 kN) to 30 kips (133.5 kN). With the beam being supported at both ends and assuming that the actuator load is transferred to two equal concentrated loads equally spaced from the ends, the moment at each strain gauge location along the length of the beam was determined. Referring to Figure 3, strain gauges 1 and 2 are located at the mid-span of the beam, which is 65 inches (165 cm) from either support. Strain gauges 3 through 8 are located 29.5 inches (75 cm) from the left support. Based on this information, the moment at 65 inches (165 cm) from the support and 29.5 inches (75 cm) from the support was determined under various loadings. Theoretical strain was determined using beam bending theory equations and an assumed modulus of elasticity of 29,000 ksi (200,000 MPa). Equations used to determine theoretical strain include:

$$\sigma = \frac{Mc}{I} \tag{1}$$

$$\varepsilon = \frac{\sigma}{E}. \tag{2}$$

The correlation between measured and theoretical strains are shown in Figure 5. It can be observed that strain gauges 1, 2, and 4 compare well to theoretical expectations with a percent error between 0 to 10% with strain gauge 3's measured strain varies from the expected theoretical value by 8 to 18.5%. A summary of percent errors for each gauge is summarized in Table 1.

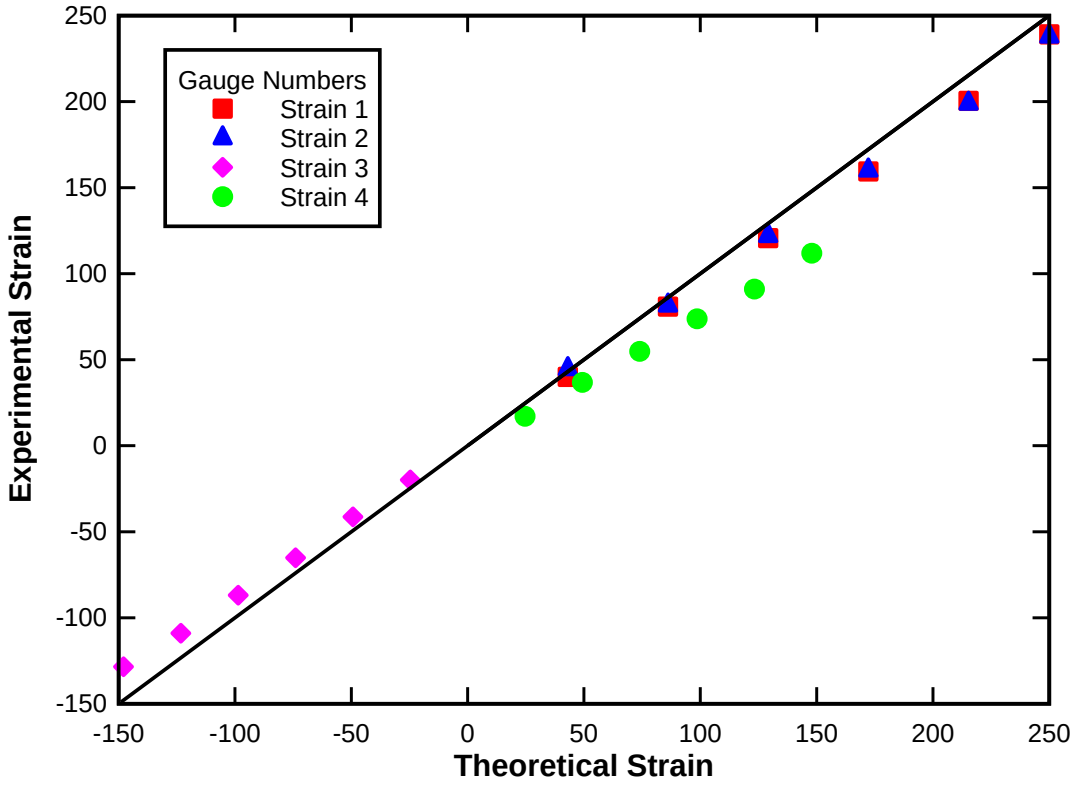

Figure 5: Correlation between theoretical and experimental strains (Mcconnell, et al. 2014)

Table 1: Percent errors between theoretical and experimental strain for gauges 1-4

	Strain Gauge Number			
Load (kips)	**1**	**2**	**3**	**4**
5	1.31	10.22	8.10	7.11
10	0.36	0.63	12.31	0.06
15	0.84	0.31	17.91	0.74
20	1.74	1.29	17.96	0.18
25	1.18	1.87	18.43	1.06
30	1.76	2.21	16.31	1.29

In order to evaluate the response of gauge 3, the strain profile through the instrumented cross-section in the undisturbed region was created from the strain gauges 3, 4, 5, and 6 data. Strain gauge 6 is the axial strain from the strain rosette. As can be seen in Figure 6, a linear strain distribution is obtained at each level of loading, which is proven by a linear curve-fit producing R^2 values between 0.9924 and 0.9995. However, Figure 6 also depicts that the neutral axis (n.a.) in this region of the beam is not observed at mid-height of the cross-section which would be expected based on pure bending theory. The offset Δ is 0.72 in (1.83 cm).

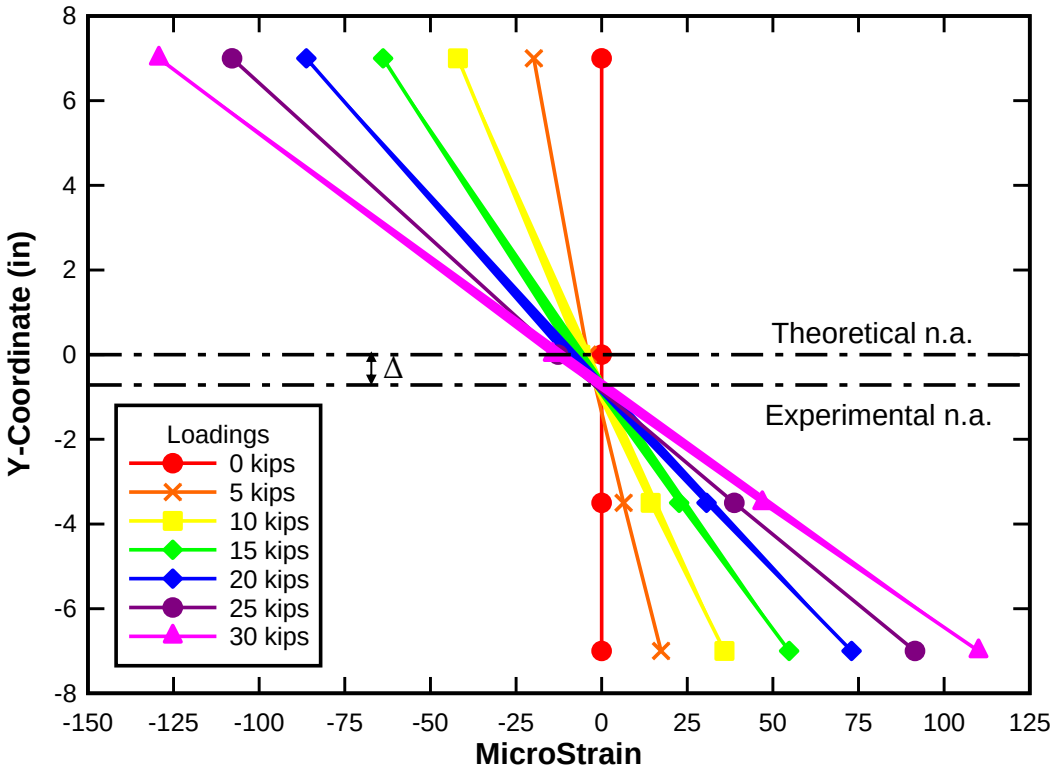

Figure 6: Strain profile obtained from strain gauges 3 – 6 throughout the loading range (Mcconnell, et al. 2014)

To further evaluate the neutral axis being at a height lower than mid-height of the beam, the condition of the beam was further analyzed. Firstly, from previous tests being conducted on the specimen, forty $\frac{7}{8}$ inch (22.25 mm) holes had been drilled in the top flange, twenty per side. When calculating the neutral axis based on a cross-section with the holes drilled out, as seen in Figure 7, the neutral axis shifts from 7 inches (17.8 cm) from the bottom of the bottom flange to 6.57 inches (16.7 cm) from the bottom flange. This causes a 6.3% difference between the undrilled and drilled cross sections. Further, by measuring and comparing the largest vertical distance between either edge of top and bottom flanges to the floor, one can determine whether the flanges of the lab specimen, a W14x87 (W350x129) beam, were out of square. According to the American Institute of Steel Construction and based on Figure 8, AISC (2014) Table 1-22 entitled "ASTM A6 Tolerances for W-Shapes," says that for a cross-section with a nominal depth greater than 12 inches (30.5 cm), the maximum permissible $T + T'$ for flanges out of square is $\frac{5}{16}$ inches (7.94 mm). For the lab specimen, the $T + T'$ value measured is $\frac{5}{16}$ in (7.94 mm), which is right on the tolerance limit, but the cross-sectional variation of the lab specimen is permitted. The obvious camber in the beam is then quantified. According to the same AISC (2014) Table 1-22, for a beam with flange width of 14.5 in (36.8 cm), the permissible variation in straightness for camber, in inches, is calculated by the following equation:

$$\frac{1}{8}\ in\ \times \frac{total\ length, ft}{10} \tag{3}$$

For the lab specimen, the permissible camber is $\frac{5}{32}$ of an inch (3.97 mm). The measured camber in the specimen, relative to the floor, is $\frac{3}{16}$ of an inch (4.76 mm), $\frac{1}{32}$

inches (0.794 mm) more than the tolerance for this uncambered section. Likely reasons for the unexpected neutral axis location is the presence of drilled holes in the top flange, nearly exceeded rotation limits of the flanges, and exceeded camber tolerances in the lab specimen.

To conclude, the highly consistent axis location and linear strain distribution indicates that LORD Microstrain's strain instrumentation and WSN is functioning properly and the geometric imperfections of the lab specimen are the likely reason for an unexpected neutral axis location.

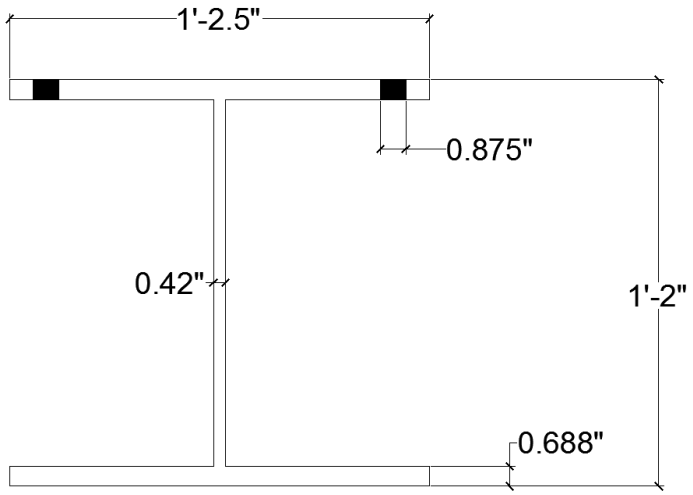

Figure 7: W14x87 Cross-section with holes drilled out on top flange

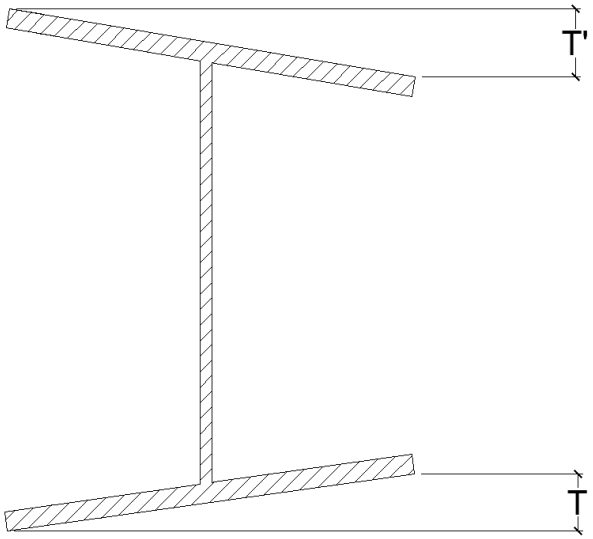

Figure 8: Variables to determine the flanges out of square AISC cross-sectional tolerance (AISC 2014)

2.4.2 Load Test 2

In order to validate the accelerometer, all data was documented for the second load test and graphed. For the single accelerometer located at the mid-span of the laboratory specimen, acceleration in the vertical direction was recorded continuously at 512 Hz. A time-history plot of the data collected from the accelerometer is shown in Figure 9. Figure 10, Figure 11, and Figure 12 show the time-history plot of the 0.5 Hz, 1 Hz, and 2 Hz respectively. From this figure, the increasing peaks of acceleration match the increasing frequency patterns induced to the beam.

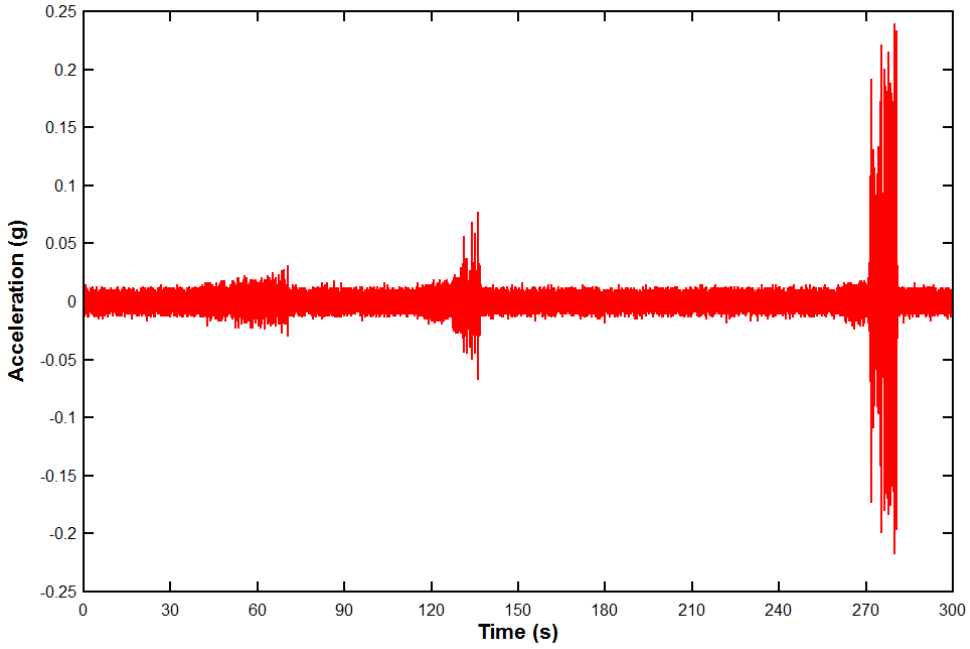

Figure 9: Raw data obtained from the accelerometer for load test 2

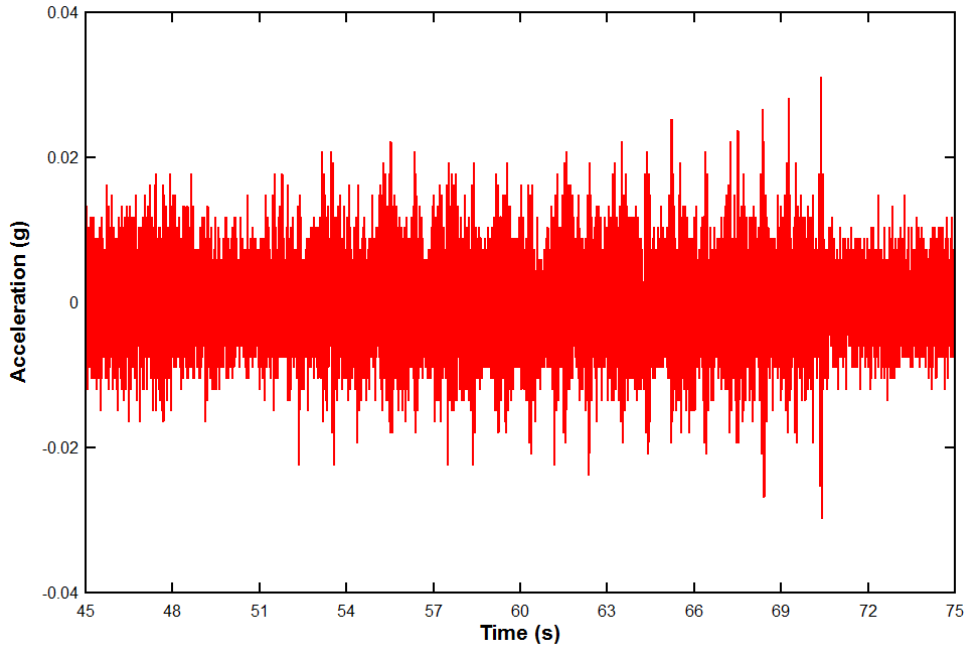

Figure 10: 0.5 Hz Portion of Load Test 2

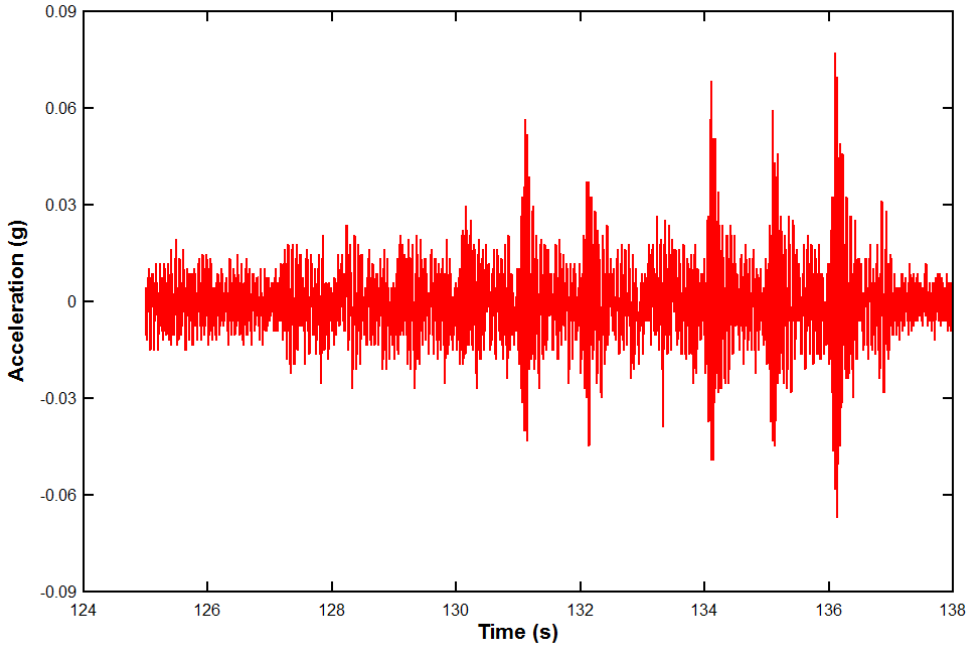

Figure 11: 1 Hz Portion of Load Test

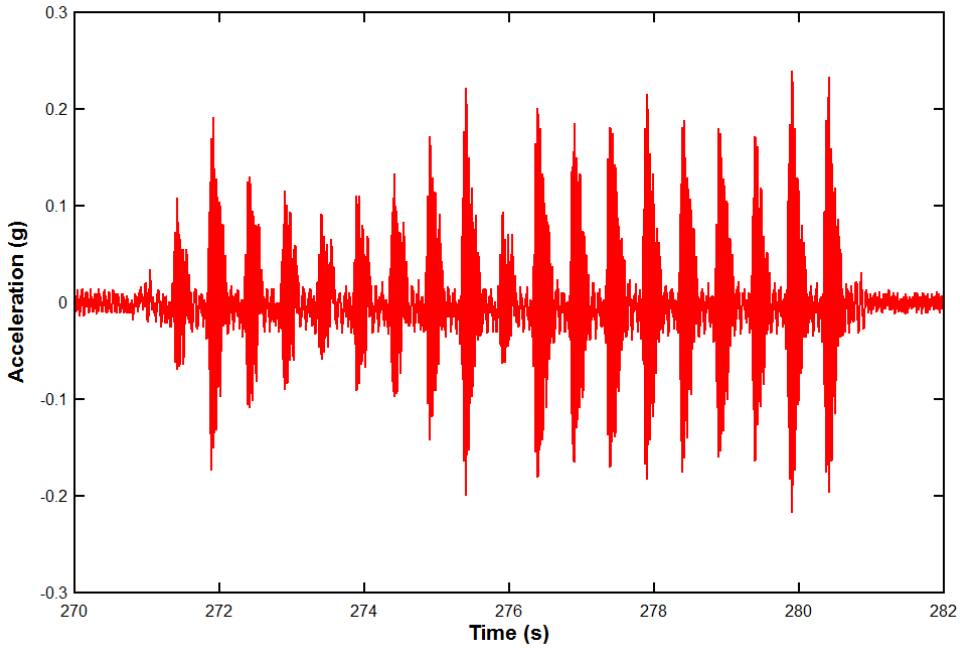

Figure 12: 2 Hz Portion of Load Test

In order to validate the data obtained in Load Test 2, a Fast Fourier Transform (FFT) analysis was conducted to see if the frequency peaks match the frequencies of the load cycles. The FFT is shown in Figure 13. The peaks of the FFT coincide with the frequencies of 0.5 Hz, 1 Hz, and 2 Hz tested in Load Test 2. Table 2 compares the peak values of the FFT plot with the actual testing frequencies. All of the percent differences were less than 1%. The accurate frequency readings validate the WSN due to the low percent differences.

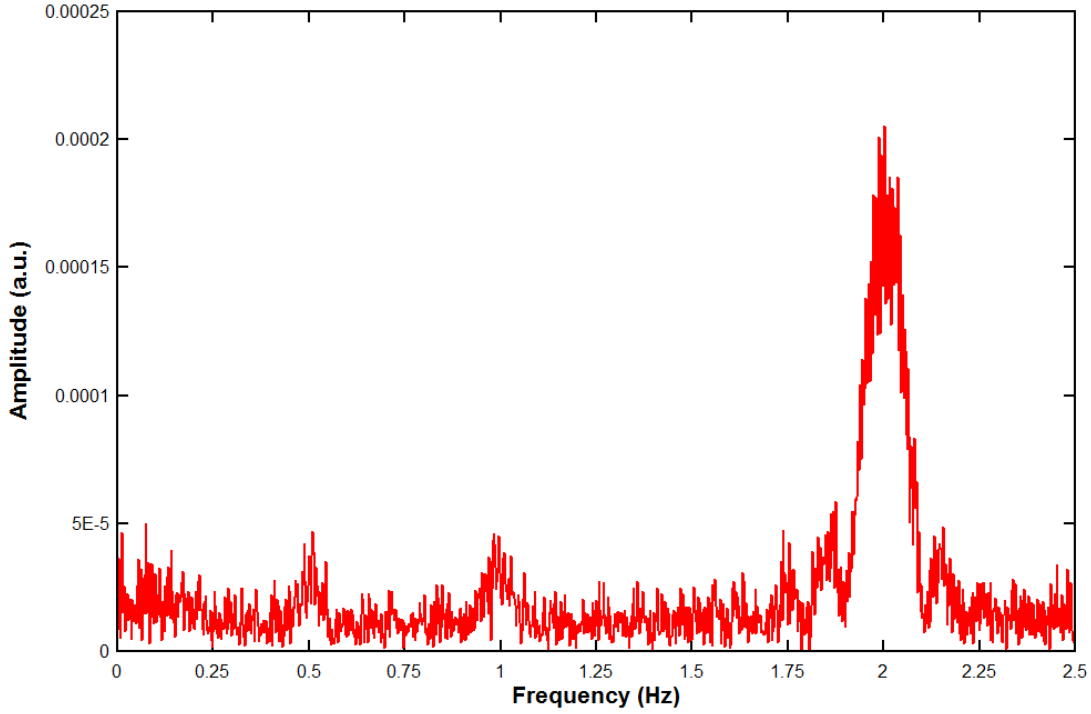

Figure 13: FFT of Load Test 2 with peaks at 0.5 Hz, 1 Hz, and 2 Hz

Table 2: Summary and comparison of frequencies obtained in the FFT plot versus the frequencies tests.

	FFT Frequency at Peak Amplitude (Hz)	Percent Difference
Peak 1 (0.5 Hz)	0.5098	0.97%
Peak 2 (1 Hz)	0.9824	0.89%
Peak 3 (2 Hz)	2.0020	0.05%

2.4.3 Load Test 3

For the impact test, acceleration was recorded with the wireless accelerometer node and then compared with a high-precision capacitive accelerometer. The impact test was carried out and an FFT analysis was conducted for both accelerometers. The frequencies obtained from the recorded accelerations were compared in order to validate the wireless accelerometer. Figure 14 shows the compared results of the FFT for the test. Also shown in Figure 14 are the calculated natural frequencies for a simply supported beam. These frequencies are based on the instrumented steel member's properties and modes of vibration using beam theory. Eq. (4) gives the natural vibration frequencies for various modes of vibration, where "n" is the mode of vibration, "L" is the span length, "EI" is the flexural rigidity, and "m" is mass per unit length (Chopra 2012). Eq. (5) converts the angular frequency unit of radians per second to Hertz (Hz).

$$\omega_n = \frac{n^2\pi^2}{L^2}\sqrt{\frac{EI}{m}} \tag{4}$$

$$f_n = \frac{\omega_n}{2\pi} \tag{5}$$

For the steel member tested in Load Test 3, the span length is 11 ft (3.35 m), Young's Modulus is 29,000 ksi (200,000 MPa), I_x for a W14x87 (W350x129) is 967 in^4 (40,250 cm^4), and the mass per unit length for a W14x87 (W350x129) is 2.7 lbs^2/ft^2 (129.3 kg/m). With these input values, the natural frequency for various modes of vibration can be calculated. Modes of vibration 1 and 2 were determined for Load Test 3. The decision to stop after mode 2 is due to the small amplitudes of motion that would be expected for these higher modes of vibration. Also, the limits of data acquisition (sampling rate and accelerometer limits) do not allow for capturing higher modes.

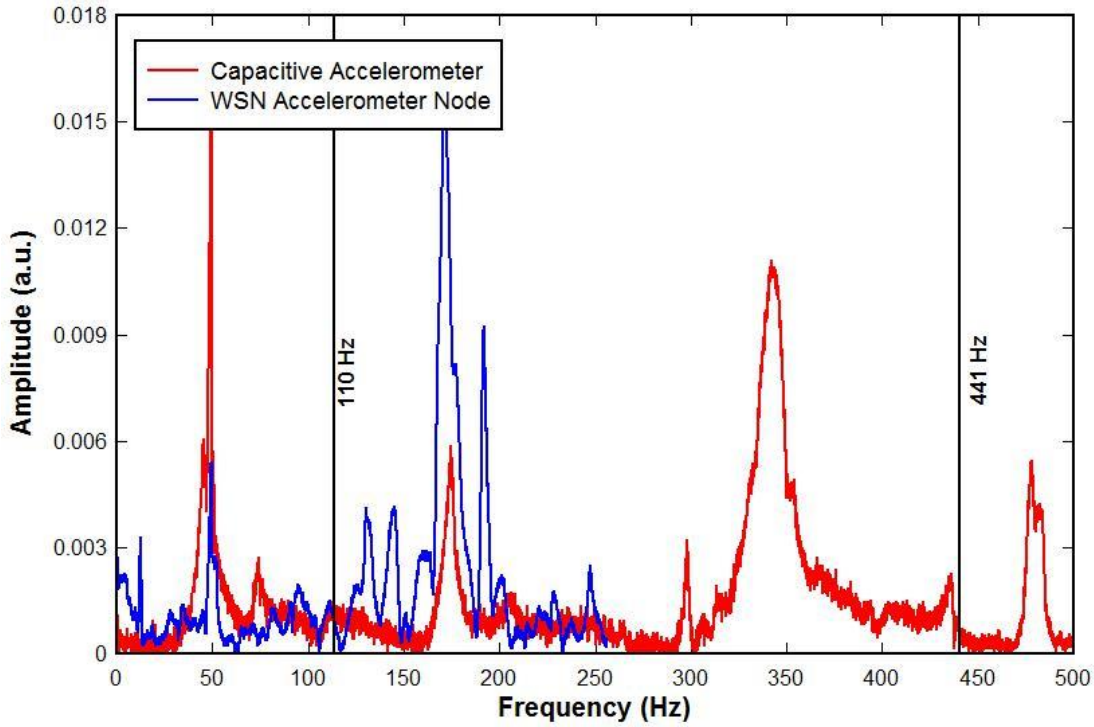

Figure 14: FFT comparison between the capacitive accelerometer and the wireless accelerometer for the first test. The vertical lines denote the calculated first and second frequencies of vibration.

Table 3 summarizes the findings of the peak natural frequencies between both accelerometers. As can be seen in the table, the largest percent difference between the two accelerometers' peak frequencies is 2.04%. The percent difference between the natural frequency and the WSN accelerometer node is 1.08%. Due to the low percent difference between the natural frequency and the WSN, the WSN's technology can be verified.

Table 3: Summary and comparison of natural frequencies obtained from both accelerometers for both tests and calculated frequencies

	Capacitive accelerometer (Hz)	**WSN accelerometer node (Hz)**	**Calculated Natural Frequency (Hz)**	**Percent Difference Between Capacitive accelerometer and WSN accelerometer**	**Percent Difference Between Natural Frequency and WSN accelerometer**
Peak 1	113.7	111.4	110.2	2.04%	1.08%
Peak 2	455.9	--	440.7	--	--

Both the WSN accelerometer node and the capacitive accelerometer show peaks at 49.5 Hz and 175 Hz; however, there is no natural frequency determined near this value. There are some likely reasons for these frequencies. Firstly, Eq. (4) and Eq. (5) determine the natural frequencies for a simply supported member. As shown in Figure 3, the laboratory specimen has two unaccounted cantilever sections on each end which will affect the calculation of the natural frequencies. Also, discrepancies can come from the assumed support pinned conditions. Eq. (4) and Eq. (5) assume a simply supported beam, which includes a pinned and a roller support. Furthermore,

the holes drilled in the top flange of the test specimen, as shown in Figure 7, could further effect the natural frequencies. Finally, some of the peaks may be associated to torsional modes, which were not calculated. The 49.5 Hz peak and the 175 Hz peak present in both data sets could be a natural mode of vibration associated with the location of the beam supports. For the peaks near 49.5 Hz, the difference between frequencies measured by the accelerometers is 0.56%. For the peak near 175 Hz, comparing the capacitive accelerometer peak to the WSN accelerometer node peak to one another leads to a percent difference of 1.91%.

Comparing the measured frequencies between the capacitive accelerometer and the WSN accelerometer node have a maximum percent difference of 1.91%; and, the percent difference is more accurate to examine since it is comparing the frequency of the laboratory specimen rather than a theoretical model. Although, the average percent difference between the two measured accelerometers validates the wireless accelerometer, an explanation for the additional frequency peaks should be investigated in the future.

Chapter 3

IN-FIELD PROCEDURE

3.1 Selection of Building Members to be Instrumented

The ultimate objective of this thesis is to successfully implement a wireless sensor network (WSN) during construction in order to quantify peak strains of a building during construction. It was therefore necessary to instrument a steel building to determine the history of construction-induced stresses. The site of the construction monitoring is an addition to an existing building located on the University of Delaware campus in Newark, DE. The addition will include four floors and will contain mainly office space and conference rooms. The structural steel members chosen for in-field WSN instrumentation are highlighted in Figure 15. The columns picked include 3C3 and 24C3, and the beams are 28B1, 25B2, and 28B4, which are all depicted in Figure 15. Situations where actual stresses a steel member experiences are predicted less confidently during construction when field conditions, fit-up problems, and temporary loadings may differ from the designer's expectations and in the vicinity of connections. Once the building is monitored during construction, finding the peak strains a member experiences is wanted. As a result, the data collected from instrumentation of a building, will provide the foundation for determining less known construction and connection stresses of a steel member.

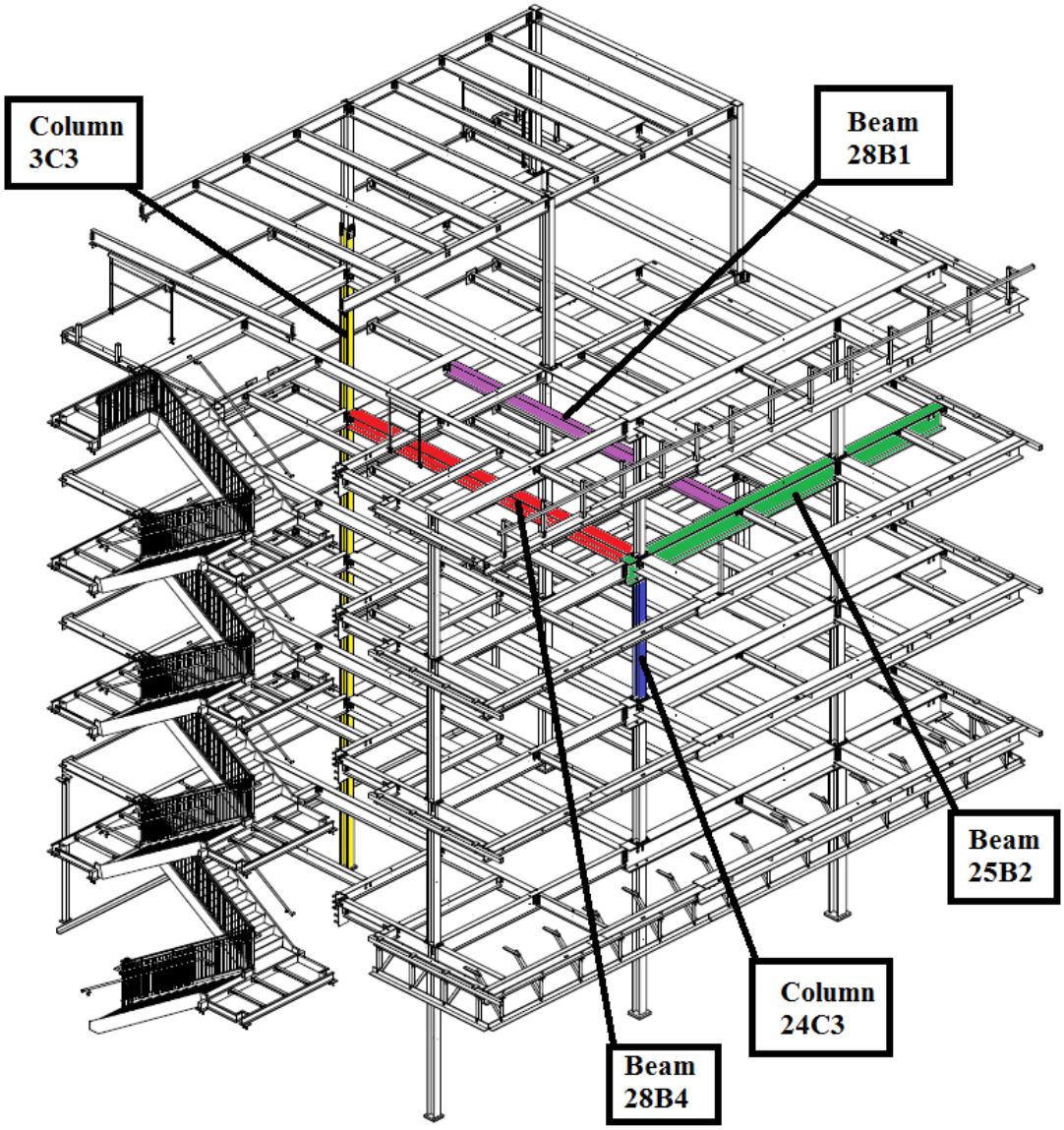

Figure 15: Isometric view of instrumented building with labeled structural steel members (Adapted from R.C. Fabricators Inc.)

3.2 Instrumentation of Selected Members

In order to collect strains of steel members during construction, the members highlighted in Figure 15 were instrumented prior to building erection. The strain

gauges were attached to the steel members at R.C. Fabricators Inc. (RCF) in Wilmington, DE before they were shipped to the construction site. Weldable strain gauges were used. Figure 16 and Figure 17 are pictures of the instrumentation for member 3C3. Similar instrumentation was conducted for all other members. The WSN was also setup in sleep mode at RCF. Once the WSN was within range of the construction site, it could be woken in order to collect data. The gauges were therefore able to collect data beginning as the members were unloaded from the delivery truck.

Figure 16: Instrumenting member 3C3 at RCF with weldable strain gauges and WSN nodes

Figure 17: Final instrumentation of the steel members for Purnell Hall

For a steel member in a building, actual stresses are predicted less confidently in the vicinity of connections. This is due to induced local stress concentrations. Therefore, a majority of the strain gauges were located near connections on the members. In total, 40 strain gauges and 10 WSN nodes were implemented, which comes to two nodes and eight gauges per beam. Table 4 outlines which nodes contain which gauges. "G" represents a strain gauge and "R" represents a single strain gauge in a strain rosette. The exact gauge and node layout can be seen in Appendix A. The gauge locations focused on bolted connections where various members were assembled. These gauges in the vicinity of a certain connection are referenced as sets. A set contains two to six gauges near a corresponding connection. Table 5 outlines the 22 sets created for Purnell Hall. The sets instrumented are used to determine peak strains and corresponding strains at the other gauge locations.

Table 4: Gauges per node and corresponding member

Node	Gauge	Gauge	Gauge	Gauge	Member
30343	G1	G2	G3	G4	3C3
30344	G9	G10	G11	G12	24C3
33201	G18	G19	G20	G21	25B2
35376	R10	R11	R12	G24	28B4
35385	R4	R5	R6	G22	28B1
35386	R7	R8	R9	G23	28B1
35387	G13	G14	G15	G16	24C3
35389	G25	G26	G27	G28	28B4
35392	R1	R2	R3	R4	25B2
35393	G5	G6	G7	G8	3C3

Table 5: Sets of gauges in the WSN for Purnell Hall

Set Number	Gauge	Gauge	Gauge	Gauge	Gauge	Gauge
1	G1	G5	G6	---	---	---
2	G2	G7	G8	---	---	---
3	G3	G4	---	---	---	---
4	G1	G2	G3	---	---	---
5	G9	G13	G14	---	---	---
6	G12	G15	G16	---	---	---
7	G9	G10	G11	G12	---	---
8	R1	G19	---	---	---	---
9	R1	R2	R3	---	---	---
10	G18	G19	---	---	---	---
11	R1	G18	G19	---	---	---
12	G17	G20	G21	---	---	---
13	G22	G23	---	---	---	---
14	R4	R5	R6	---	---	---
15	R7	R8	R9	---	---	---
16	R4	R5	R6	R7	R8	R9
17	R10	G25	---	---	---	---
18	R10	R11	R12	---	---	---
19	G25	G26	---	---	---	---
20	R10	G25	G26	---	---	---
21	G27	G28	---	---	---	---
22	G24	G28	---	---	---	---

3.3 WSN Collection Details

Data collection at Purnell Hall started on November 3, 2014 and ended on December 20, 2014. Data collection started when the steel members were delivered to the site and continued until fireproofing was about to occur. The WSN was powered by two D sized batteries which have 18,000 mAh capacity each, totaling 36,000 mAh per node. According to Figure 18, the WSN can sample a four-channeled 350 Ω node at 16 Hz for 3,100 hours, or 129 days. Therefore, initial strain gauge sampling of the WSN occurred continuously for 24 hours a day 7 days a week.

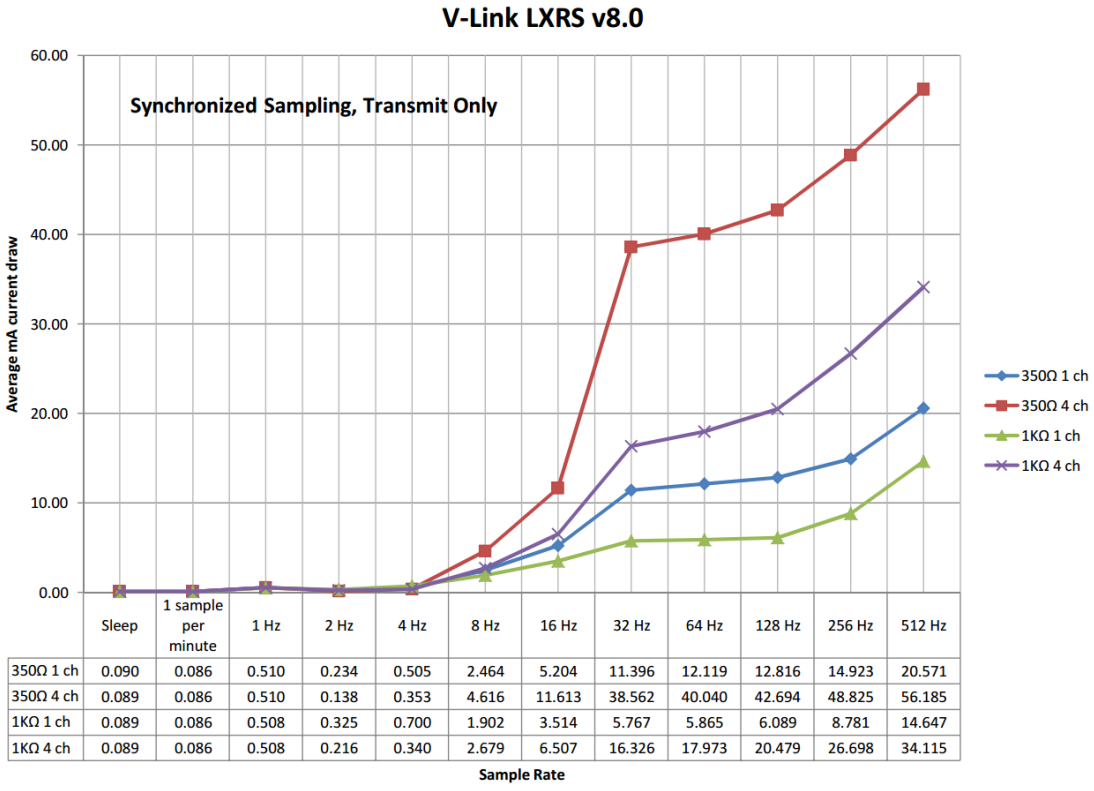

	Sleep	1 sample per minute	1 Hz	2 Hz	4 Hz	8 Hz	16 Hz	32 Hz	64 Hz	128 Hz	256 Hz	512 Hz
350Ω 1 ch	0.090	0.086	0.510	0.234	0.505	2.464	5.204	11.396	12.119	12.816	14.923	20.571
350Ω 4 ch	0.089	0.086	0.510	0.138	0.353	4.616	11.613	38.562	40.040	42.694	48.825	56.185
1KΩ 1 ch	0.089	0.086	0.508	0.325	0.700	1.902	3.514	5.767	5.865	6.089	8.781	14.647
1KΩ 4 ch	0.089	0.086	0.508	0.216	0.340	2.679	6.507	16.326	17.973	20.479	26.698	34.115

Figure 18: WSN Power Profile (LORD MicroStrain)

All ten nodes were configured exactly the same. Four strain gauge channels and one temperature channel were enabled per node. Synchronized sampling occurred at 16 Hz. The transmit power level, which determines the power consumption and wireless communication range between gateways and the nodes, was set to the extended range, which outputs about 39 mW and can measure within 1.25 miles (2 km). Even though the laptop with the gateway was setup in Purnell Hall, it was determined that the construction equipment and amount of steel onsite made it difficult to obtain a strong communication signal. The higher power transmission levels aided in increasing the reliability of communication.

As continuous sampling occurred through the construction stage, communication errors began occurring. It was decided to stop recording through the night and only sample during the construction hours of the project. This gave better results during the construction hours while also conserving batter life.

3.4 Camera Specifications

For the video recording of the construction site, a UI-1540SE model camera by Imaging Development Systems (IDS) GmbH, as seen in Figure 19, was used. The construction site was monitored during daylight hours while the nodes were collecting data. Therefore, the camera was monitoring the construction site from November 3, 2014 until December 20, 2014 during construction hours. The camera was set up on a tripod in Smith Hall, which is an adjacent building to Purnell Hall on the University of Delaware Campus. The camera's view can be seen in Figure 20. Having video recordings of the construction site allows to visually determine what construction practices may cause large strain readings.

Figure 19: IDS Camera model UI-1540SE that was used for video documentation of the construction site

Figure 20: View of Purnell Hall's construction site from the camera

3.5 In-Field Data

On the morning of November 3, 2014, the steel member 3C3 was delivered to the Purnell Hall construction site. Other steel members 24C3, 28B1, 25B2, and 28B4 were delivered on November 7, 2014. As soon as the delivery truck was in range of the WSN, the nodes were turned off of sleep mode and data collection began. This was around 9:00am. Data collection continued until December 20, 2014. An example of the outputted data collected by the WSN can be seen in Figure 21.

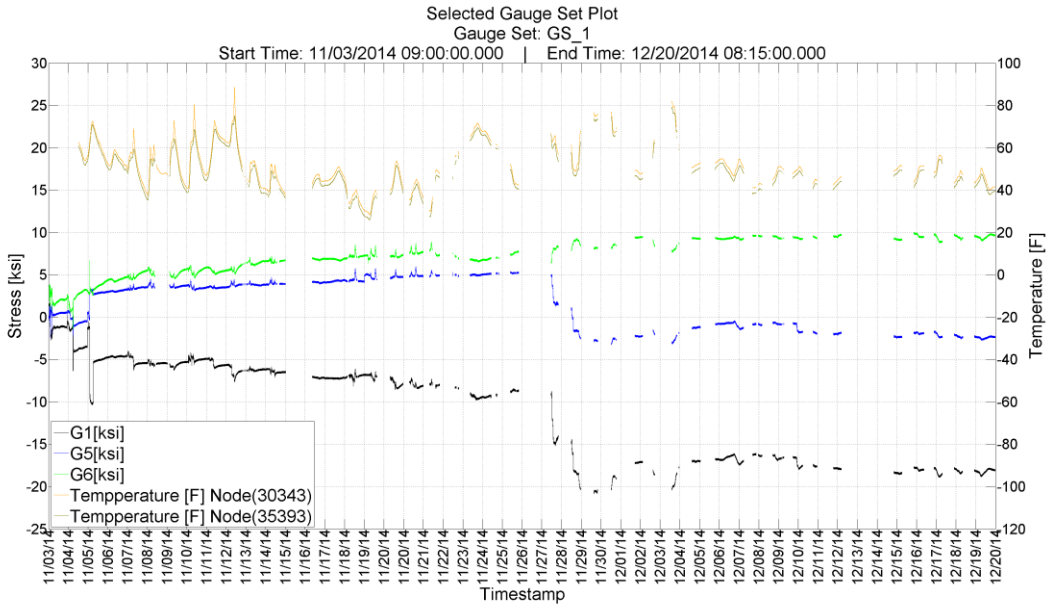

Figure 21: Data Collection for Gauge Set 1

Figure 21 shows the data collection for Gauge Set 1, which includes strain gauges G1, G5, and G6 located at the base of column 3C3 and temperature gauges. All other gauge set graphs showing the entire data collection can be seen in Appendix B. Time vs. stress and time vs. temperature are both represented. Issues with

operating the Node Commander program occurred on November 15, 2014, November 26, 2014, and December 13, 2014. Henceforth, the data collected during those periods was unreliable and thus excluded from graphical representation which is consistent with all gauge sets. For the first half of data collection, the strain gauges were operated 24 hours a day. For the second half of the data collection, the strain gauges were only operated during the day or when the construction crews were on site. This creates a line with breaks since no data collection during the night occurred. Turning the strain gauge collection off conserved battery and allowed for smaller files to be analyzed. Strain after November 28, 2014 was moderately constant and we therefore concluded it was acceptable to only collect data during the day.

Chapter 4

RESULTS AND DISCUSSION

4.1 Collected Data Results

The time history of the stresses the members 3C3 and 24C3, 28B1, 25B2, and 28B4 experience are shown in Appendix B. However, in order to verify that the steel members did not reach yield stress, it is important to examine times when peak stresses occurred. During times of peak stresses, it is important to understand how the member is reacting. Therefore, analyzing how gauge sets react during times of peak stresses is important.

In order to further analyze the strain collected, the maximum strain was found for a single gauge and then converted to stress using Eq. (2). The respective maximum stress and timestamp that the maximum stress occurred was noted. At that particular timestamp, all other gauges in the gauge set's stress are noted as well. Gauge sets are grouped together in order to most effectively encompass a connection of a member or a member in general. Thus, it is useful to know what the other strain gauges are measuring when a particular strain gauge is experiencing its maximum. Table 6 shows each set's absolute maximum gauge and the corresponding gauges' stresses at that time. Appendix C breaks down this information by showing the maximum positive (= tension) and negative (= compression) stresses. All peak stresses are absolute values, which were inferred from the measured strain by using Eq. (2).

Table 6: Gauge stresses at time of absolute maximum stress for all gauge sets (absolute values)

ABSOLUTE MAXIMUM STRESSES			
SET NUMBER	**DATE/TIME**	**GAUGES IN SET**	**PEAK STRESS**
1	11/30/2014 14:30:34.324	**G1**	**-20.8529**
		G5	-2.8549
		G6	8.1735
2	12/19/2014 13:05:19.449	**G2**	**-14.6883**
		G7	-1.7535
		G8	7.3571
3	11/03/2014 10:40:21.699	**G3**	**12.1405**
		G4	-1.1991
4	11/30/2014 14:30:34.324	**G1**	**-20.8529**
		G2	-13.8551
		G3	-5.1203
5	11/29/2014 07:24:38.324	**G9**	**-21.2698**
		G13	11.1981
		G14	16.5755
6	12/04/2014 15:31:19.137	G12	-0.9383
		G15	**-20.0495**
		G16	-11.5099
7	11/29/2014 07:24:38.324	**G9**	**-21.2698**
		G10	-15.0029
		G11	-2.4317
		G12	6.7623
8	11/19/2014 09:08:21.949	**R1**	**8.5916**
		G19	5.7850
9	11/30/2014 14:28:47.637	R1	4.7832
		R2	-7.2935
		R3	**-11.5042**
10	11/29/2014 18:22:34.012	G18	2.4699
		G19	**6.0274**
11	11/19/2014 09:08:21.949	**R1**	**8.5916**
		G18	2.4727
		G19	5.7850
12	11/14/2014 09:12:21.637	G17	1.9989
		G20	**-9.2988**
		G21	0.5797
13	12/11/2014 12:07:10.012	G22	10.4414
		G23	**18.8928**
14	12/01/2014 08:23:50.762	**R4**	**-4.0705**
		R5	-2.4012
		R6	-0.7483

Table 6: Continued

15	11/07/2014 14:32:28.824	**R7**	**26.1682**
		R8	20.7616
		R9	21.6321
16	11/07/2014 14:32:28.699	R4	0.7124
		R5	1.2704
		R6	1.3149
		R7	**26.1682**
		R8	20.7336
		R9	21.6546
17	11/22/2014 08:48:27.137	**R10**	**4.9942**
		G25	0.3580
18	11/22/2014 08:48:27.137	**R10**	**4.9942**
		R11	4.0872
		R12	2.7112
19	12/01/2014 08:51:19.262	**G25**	**-3.1218**
		G26	0.3766
20	11/22/2014 08:48:27.137	**R10**	**4.9942**
		G25	0.3580
		G26	-0.0373
21	12/12/2014 07:37:51.762	**G27**	**5.0941**
		G28	-0.7509
22	11/13/2014 09:00:09.012	**G24**	**-8.9752**
		G28	0.6902

4.2 Frequency of Absolute Maximum Stress

A histogram showing the frequencies of the maximum stresses of Table 6 is shown in Figure 22. Scott's normal reference rule, as seen in Eq. (6), was used to determine the bin width for the histogram.

$$h = \frac{3.5\hat{\sigma}}{n^{1/3}} \tag{6}$$

Scott's normal reference rule is optimal for random samples of normally distributed data since it minimizes the integrated mean squared error of the density

(Scott 1992). In Eq. (6), "$\hat{\sigma}$" is the sample standard deviation of the maximum stresses, "n" is the total number of gauges, and "h" is the suggested bin width. For the absolute peak stresses, "$\hat{\sigma}$" is 6.75 ksi (46.54 MPa), "n" is 40 gauges, and based on these numbers, the calculated suggested bin width "h" is 6.91 ksi (47.65 ksi).

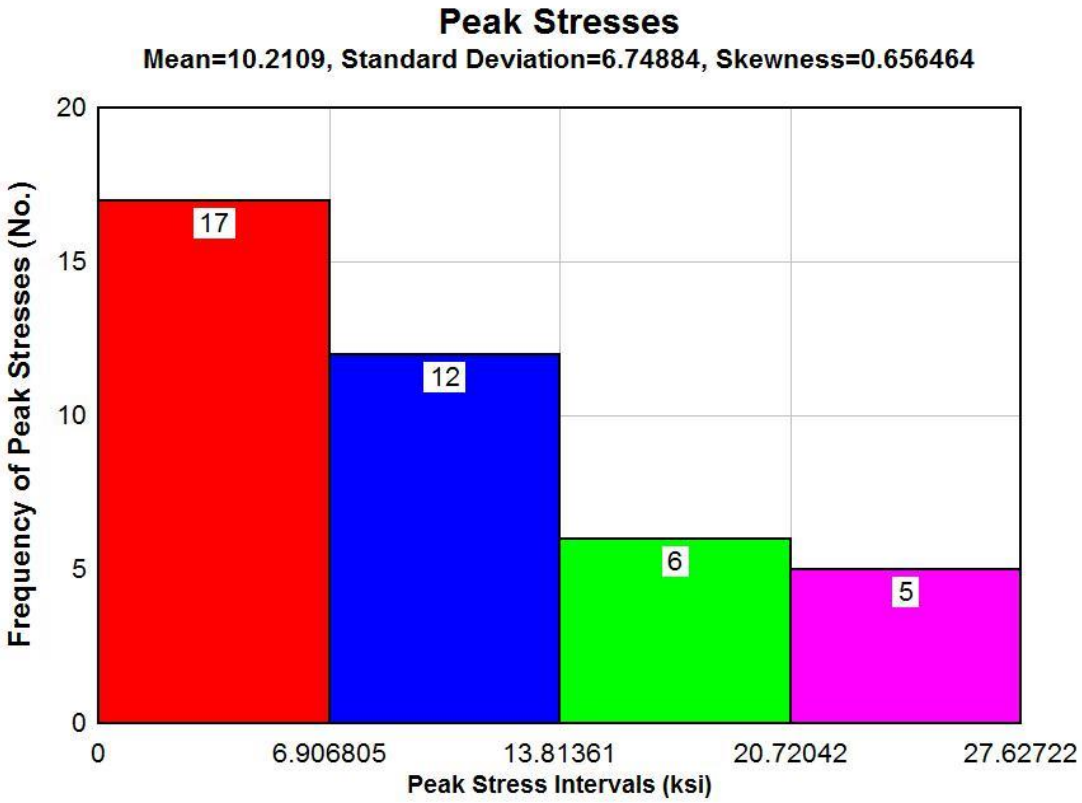

Figure 22: Histogram showing the frequency of peak stresses the steel members of Purnell Hall experience during construction

The histogram in Figure 22 is skewed to the right. Therefore, a majority of the peak stresses the instrumented steel members experience during the construction of Purnell Hall are below the mean peak stress. The maximum stress experienced by the

instrumented steel members was 26.2 ksi (180.6 MPa). This occurred in gauge R7 which is a horizontal gauge on beam 28B1 near a bolted connection. Steel plates are typically constructed from A36 steel, which means that the steel's minimum yield strength is 36 ksi (284.2 MPa). Therefore, since the maximum recorded stress of 26.2 ksi (180.6 MPa) is less than steel's yield strength of 36 ksi (180.6 MPa), the WSN validated that steel members did not yield during construction.

Chapter 5

CONCLUSIONS

5.1 Conclusions

The objective of this thesis was to evaluate and implement a WSN system during construction of a building in order to capture peak strains of steel members. This information will allow gaining insight into the stresses steel members undergo during construction and whether their strength limits are exceeded.

In order to assess the impact that construction forces have on a steel member, an investigation verifying the accuracy of a WSN was undertaken. Through analysis of theoretical versus measured strains for multiple load cases, it was proven that the WSN accurately captured the strains an instrumented member experiences and may therefore be utilized for in-field experiments.

It is important to note that this study did not look at the effect of temperature on steel members. This would need to be done in order to determine the effect of temperature on the measured strain independently from the construction effects on the measured strain. This can be done by adding temperature gauges to the regular strain gauges.

Utilizing the validated WSN to capture the forces during construction a steel member experiences verified that the yield strength of 36 ksi (180.6 MPa) for A36 steel was not reached. This is the first step in proving that the reuse of structural steel for buildings is a structurally-sound engineering practice.

5.2 Future Work

5.2.1 Laboratory Experiment to Verify In-Field Data

Once the building is monitored during construction, replicating large stresses gathered from field instrumentation in the laboratory is desired. Replication of the construction forces a typical steel member connection experiences in the field will be performed in the UD Structures Laboratory. As a result, this lab setup, accompanied by the data collected from instrumentation of a building, will provide the foundation for determining less known construction and connection stresses of a steel member.

5.2.1.1 Selection of Laboratory Specimens

After monitoring the construction forces the structural steel member experience, member 28B4, the red beam in Figure 15, was selected for further laboratory evaluation of fit-up stresses. 28B4 is a W14x99 (W360x147) beam. The in-field instrumentation of this member can be seen in Figure 23. Since the research project is concerned with quantifying construction-induced stresses in the vicinity of typical connections, this beam was chosen because it represents a standard, repeated member for this building. Further, the geometry of this beam permits cost effective and space effective experimental laboratory tests.

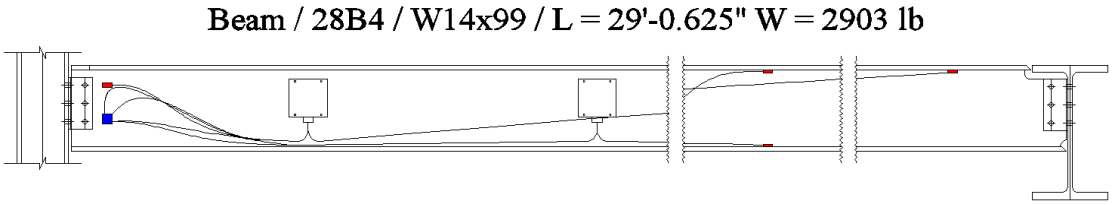

Figure 23: In-field instrumentation of structural steel member 28B4 (Courtesy: Philipp Keller)

5.2.1.2 Experimental Setup

The objective of this laboratory setup is to determine the limits of the shear connections for the beam and to replicate stresses experienced in the field. This experiment will be carried out in the University of Delaware Structures Laboratory, which already has the strong floor and the large frame test setup. The experimental setup was designed to represent the boundary conditions of members 28B4. An overview of the experimental setup can be seen in Figure 24. Due to limitations in the size of the structural laboratory, the full length of the member was not utilized. The experimental length of the member was 5 ft. For the column setup seen in Figure 24, extra steel members from the UD Structures Laboratory were used to create the column, diagonal bracing, and floor plates, as seen in Appendix D.

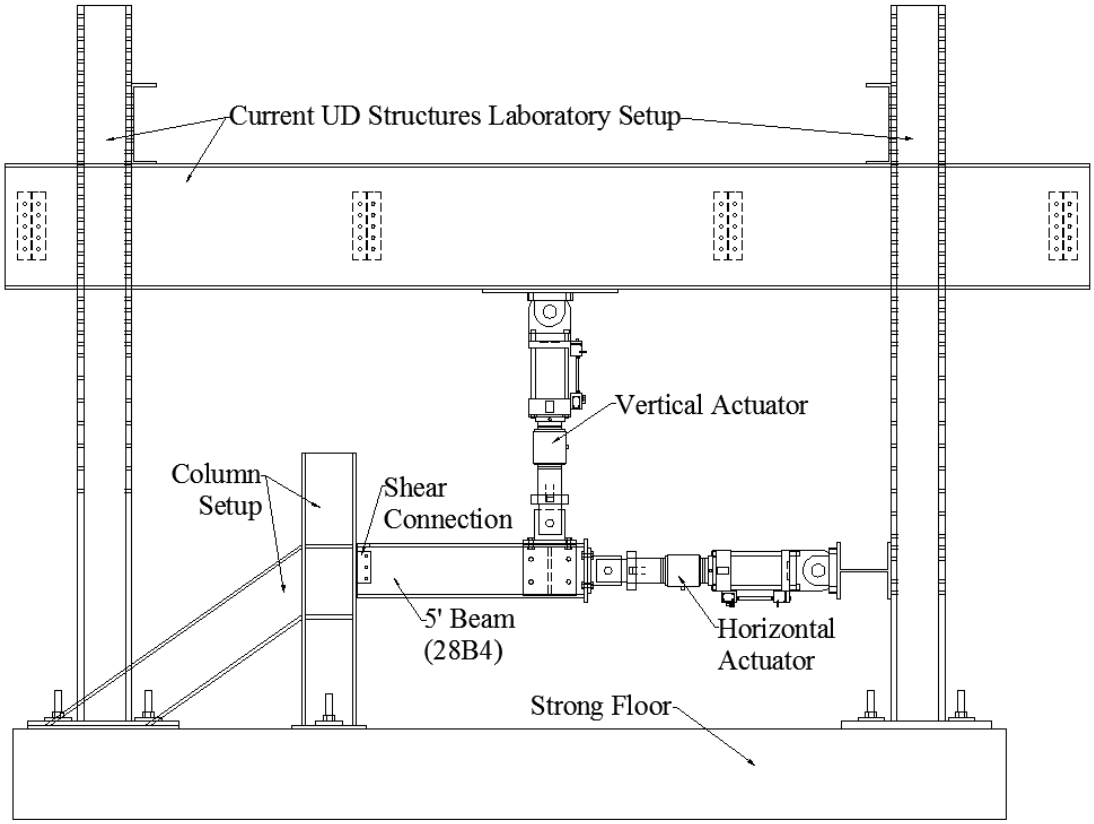

Figure 24: Experimental Setup in the University of Delaware Structures Laboratory

This experimental setup aims to replicate fit-up stresses of the shear connection for 28B4. Two 150-kip (667 kN) capacity hydraulic actuators are needed to create both axial and bending forced in the beam. The horizontal actuator, which produces the axial loading, is located at the free end of the beam. The vertical actuator, which produces the bending moments, is located 4'-3" (1.3 m) from the shear connection end of the beam. Special attachments, which connect the beam to the actuators needed to be designed. One specific design criteria was that both of the attachments must not fail prior to the shear connection for both tension and compression loadings. Failure concerns include gross section yielding, block shear, bearing strength, bolt shear, and

bolt tension for each component of both the shear connection and the actuator attachments. Each failure mode for all actuator components had to be compared to the governing failure of the shear connection in order to confirm that the failure of the shear connection will occur prior to the failure of the specimen's designed attachments. An overview of the designed attachments is shown in Figure 25 and Figure 26.

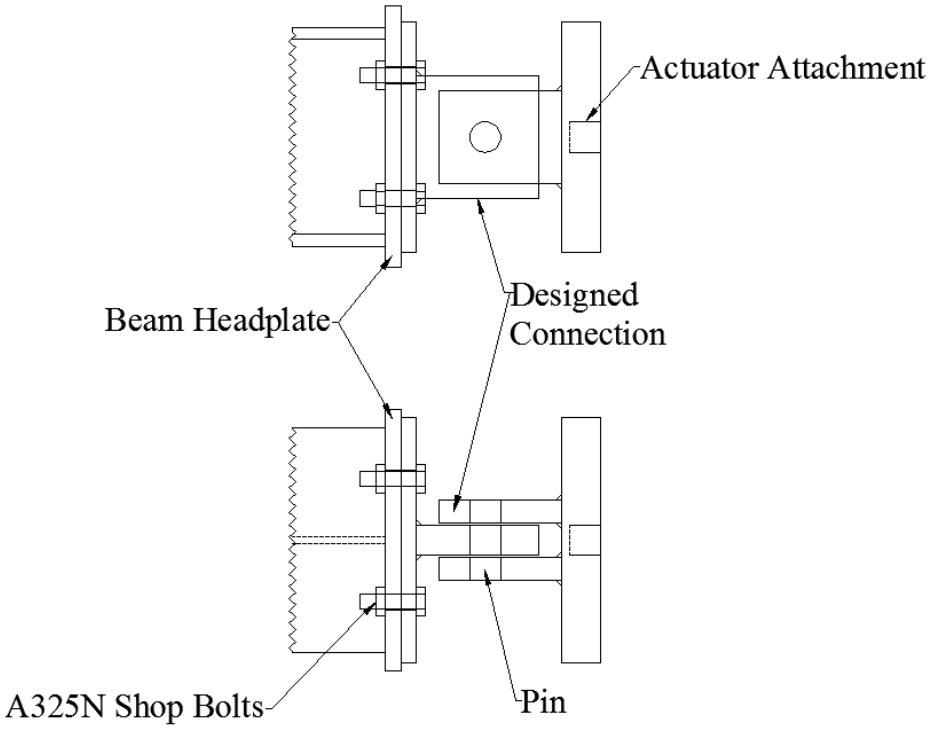

Figure 25: Horizontal actuator connection details for 28B4 (W14x99) beam

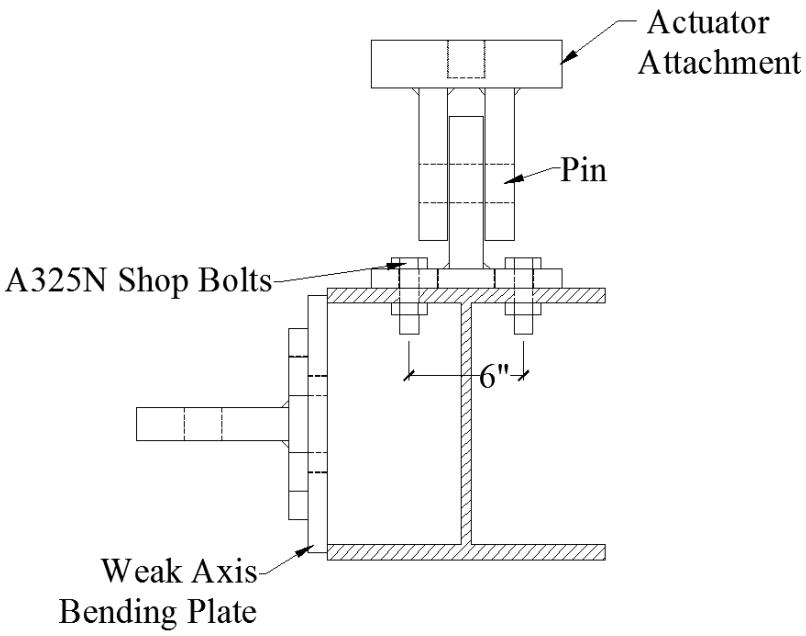

Figure 26: Vertical actuator connection details for 28B4 (W14x99) beam

An additional aspect of the experimental setup is the ability to test the beam in both strong and weak axis bending. The bolt configuration on the angles connecting the beam to the column needed to be in a square pattern so that rotating the beam for each bending scenario was achievable without drilling additional holes in the column. The angle's beam to column connection was also checked against the angle's beam web connection in order to guarantee that the failure would occur in the web of the test beam rather than in the flange of the setup column. The angle configurations for the beam are shown in Figure 27. Further, weak axis bending posed the issue of attaching the vertical actuator to the beam. This was resolved by bolting the actuator connection to a plate, and then welding this piece to the flanges. The welding will be done in the UD Structure's Laboratory after the strong axis bending tests are completed so that no additional or uneven stiffness is added to the flanges. This is shown in Figure 26.

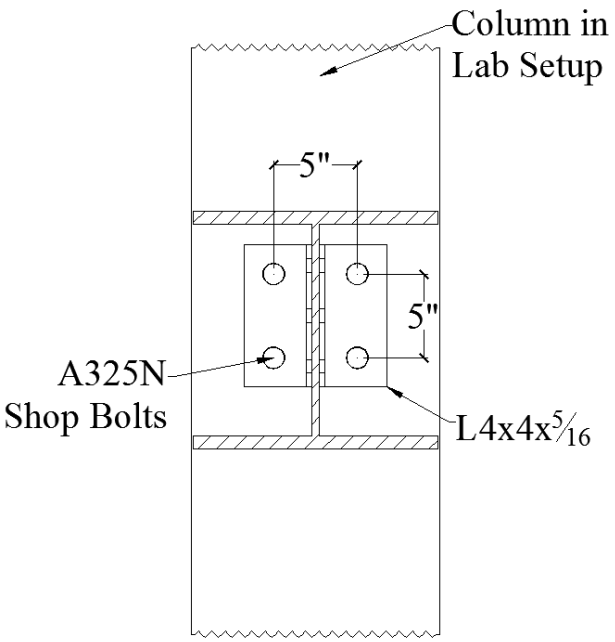

Figure 27: Angle configurations for the experimental setup

In order to reproduce and fabricate the experimental setup and laboratory specimens, new drawings using AutoCAD 2014 were created, as seen in Appendix D. These drawings were submitted to Summit Steel Inc. for fabrication. An overview of the project, which included the setup in the UD Structures Laboratory, and an overview of the components on the 28B4 beam was presented.

For 28B4 (W14x99, W360x147), a 5-ft (1.5 m) section needed to be adapted from the original full length section presented in the Purnell Hall addition drawings. The shear connection of the beam is of importance and is thus not altered for the experimental setup. The exact bolt, angle, and beam arrangements near the shear connection from the original steel fabricator drawings were utilized. For 28B4, three ¾ inch (19 mm) bolts were spaced at 3 inches (7.62 cm) on the web, 8.5 in L4x4x5/16 (L102x102x7.9) angles were utilized, and the beam had coped the flange to 8 inches

(20.32 cm). All of these details were taken from the original steel fabricator drawings. For the 5-ft (1.5 m) test beam, details near the free end of the beam needed to be added in order to facilitate actuator attachment. For the beam, four 1 in bolt holes need to be added to the top flange in order to secure the vertical actuator attachment connection. These holes are equal distance from the web centerline of the beam, and spaced evenly from the vertical actuator location of 4'-3" (1.3 m) from the connected end of the beam. A stiffener is added to support the flanges in strong axis bending and to support the welded plate in weak axis bending when loaded by the vertical actuator. The stiffener thickness is taken to be the closest quarter inch to the web thickness. At the end of each beam, a 17"x17"x1" (43cm x 43cm x 2.54cm) head plate with four 1 inch (2.54 cm) bolt holes is welded for horizontal actuator attachment. The bolt holes are centered on the head plate in an 8"x8" (20.32cm x 20.32 cm) arrangement. Each W-shape is made of A992 steel, and the angles, stiffener plates, and head plates are all constructed from A36 steel. The differences between steel types are presented in Table 7.

Table 7: ASTM specifications comparing A36 and A992 steel (McCormac and Csernak 2012)

ASTM Designation	**F_y Min. Yield Stress (ksi)**	**F_u Tensile Stress (ksi)**
A36	36	58-80
A992	50	65

The detailed drawings in Appendix D show the designed horizontal and vertical attachments which depict the bolt, weld, and plate details. Both the horizontal and the vertical actuator attachments are planned to be used for future experiments in

the University of Delaware Structures Laboratory. For each actuator, an attachment detail for the beam and for the actuator will have to be designed.

For the horizontal actuator, an attachment is bolted to the beam and then connected to the threaded actuator attachment. The horizontal attachment details, both on the beam and on the actuator, are then held together by a pinned connection which allows for rotation by a rod with holes drilled at either end for cotter pin securement. These individual parts can be seen combined in Figure 25.

For the vertical actuator, the part of the attachment that gets bolted to the beam consists of long-slotted holes which are necessary due to reusing this specimen for future tests in the Structures Laboratory. In order to satisfy the A325 bolt clearances presented in AISC's Steel Construction Manual Table 7-15, for 1 in bolts, the distance between the center of the bolt and the edge of the beam's web fillet needs to be greater than 1 inch (AISC 2014). From the same source, Table J3.4 states that for a 1 in bolt, the minimum edge distance from the center of a standard hole to the edge of the connected part is 1.25 inch (AISC 2014). Therefore, long-slotted holes needed to be utilized to satisfy these constraints between various beam flange sizes. The vertical beam attachment is held together to the threaded vertical actuator attachment by rod which simulated a pinned connection. This rod is secured by cotter pins. The combination of these individual actuator attachments can be seen in Figure 26.

5.2.1.3 Instrumentation

The specimen was instrumented with different strain sensors. To measure strains in the laboratory, uniaxial strain gauges and strain rosettes were installed. Uniaxial strain gauges measure strain in one direction. Strain gauge rosettes consist of three individual strain gauge elements which allows for the determination of principal

strains and principal directions. The strain gauge sizes used in this experiment are summarized in Table 8.

Table 8: Instrumentation specifications

	Length (in)	Width (in)	Angle (degrees)	Resistance (ohms)
Uniaxial Strain Gauges	0.250	0.120	N/A	350
Strain Gauge Rosettes	0.125	1.52	45	350

In conjunction with the strain gauges, a carbon nanotube-based (CNT) sensing skin is used in the laboratory experiment. According to Dai, Schumacher, and Thostenson (2013), an electrically percolating network, which can act as in situ damage sensors, are formed when carbon nanotubes are properly dispersed into the polymer matrix of a composite material. Strain and/or damage can be quantified by monitoring the overall electrical resistance change of the sensing composite. Thus, distributed strain measurements rather than point measurements, such as from strain gauges, are produced by these self-sensing composites. These CNT sensing skins will allow for a more accurate representation of the complex stress states around the shear connection detail. (Dai, Schumacher, Thostenson 2013)

The critical areas for this experiment are near the shear connection. Therefore, the angles and the area of the beam surrounding the connection were heavily instrumented. Each beam will have one CNT sensing skin and strain gauges are to be installed in the same locations as seen in the field plus on the angles for more detailed

data. The CNT sensing skin should be adhered on the opposite side of the web in order to compare it to the strain gauges.

5.2.1.4 Load Induction

The goal of this laboratory experiment is to understand where, why, and how the peak strains a member experienced were created. This is accomplished by working backwards from the measured strains at the connection in order to figure out what the vertical and horizontal loads were in order to create this measured strain.

5.2.2 Overall Project Future Work

The initial research described in this thesis must be further expanded in order to completely assess the potential reuse of structural steel. Future work on this project includes instrumenting steel buildings during construction and while in-service, and evaluating residual stresses in reclaimed decommissioned structural steel members.

For a structure, instrumentation will be installed and monitoring will encompass construction and then left in place to record in-service stresses. As a result, global and local construction-induced and service stresses will be quantified in the vicinity of connections. Data collected will provide information regarding whether the stresses the structural members see impair the structural integrity of the members for reuse applications.

In order to evaluate the residual stress profiles of reclaimed structural members, the shakedown theory can be used to determine the structural integrity and remaining functionality of the decommissioned members. For a structural steel member, after the yield stress is exceeded and the load is removed, there is a residual strain. Further, after repeated cycles of a load, deformation is caused in the member if

plasticity is unrestrained. Shakedown can occur because of the irreversible nature of plastic deformations. After a certain time of the cyclic loading, plastic strains stop developing any further and the application of the same cyclic loads is resisted elastically. Using this information in combination with residual stress measurements can help infer the stress state and residual strength of a member that is a candidate for reuse. The stress distribution can reveal what locations of a steel member have been subjected to stresses exceeding the yield strength. The shakedown theory can be used to validate if the existing stress state of the member is stable and whether the member can be utilized in future applications without degraded structural performance. By determining the residual stresses in decommissioned members, this research will be able to further asses the reuse potential of reclaimed structural steel members.

Each of these steps helps to create and validate analytical models which can be applied to various building configurations and construction sequences. Information such as location of structural members that experience highest stresses, spatial variability of stresses within members, and sensitivity of stress distributions to construction practices can be determined. These models will provide the opportunity to consider an even greater number of realistic scenarios so that a complete picture of the structural integrity of reused structural members will be offered.

REFERENCES

AISC. *Steel Construction Manual*. 14th ed. Chicago, IL: American Institute of Steel Construction, 2014. Print.

AISC. *Structural Steel: An Industry Overview*. Publication no. F123.v3. American Institute of Steel Construction, n.d. Web. 03 Feb. 2015.

Anastasi, Giuseppe, Giuseppe Lo Re, and Marco Ortolani. "WSNs for structural health monitoring of historical buildings." *Human System Interactions, 2009. HSI'09. 2nd Conference on*. IEEE, 2009.

Catalli, Vince, and Maria Williams. "Designing for Disassembly." *Canadian Architect*. Royal Architectural Institute of Canada, 01 Jan. 2001. Web. 20 July 2014.

Chacón, R., F. Guzmán, E. Mirambell, E. Real, and E. Oñate. "Wireless sensor networks for strain monitoring during steel bridges launching." Structural Health Monitoring 8.3 (2009): 195-205.

Cho, Soojin, Chung-Bang Yun, Jerome P. Lynch, Andrew T. Zimmerman, Billie F. Spencer Jr., and Tomonori Nagayama. "Smart wireless sensor technology for structural health monitoring of civil structures." International Journal of Steel Structures 8.4 (2008): 267-275.

Chopra, Anil K. "Systems with Distributed Mass and Elasticity." Dynamics of Structures: Theory and Applications to Earthquake Engineering. Boston: Prentice Hall, 2012. N. pag. Print.

Connor, Jerome J., A. Wada, M. Iwata, Y.H. Huant. "Damage-controlled structures. I: Preliminary design methodology for seismically active regions." *Journal of Structural Engineering* 123.4 (1997): 423-431

Dai, H. B., T. Schumacher, and E. T. Thostenson. "Carbon nanotube-based sensing composites for structural health monitoring of civil infrastructure using non-woven fabrics." *Integrative Treatment of Hypertension: A Clinical and Mechanistic Approach* (2013): 299.

Durmisevic, E., and N. Noort. "Re-use potential of steel in building construction." *DECONSTRUCTION AND MATERIALS REUSE, 0* (2003): 352-361.

EPA. *Inventory of U.S. Greenhouse Gas Emissions and Sinks: 1990-2011*. Rep. no. EPA 430-R-13-001. N.p.: n.p., n.d. *National Greenhouse Gas Emissions Data*. EPA: United States Environmental Protection Agency, 11 Apr. 2013. Web. 12 Apr. 2014.

Farrar, Charles R., and Keith Worden. "An introduction to structural health monitoring." *Philosophical Transactions of the Royal Society A: Mathematical, Physical and Engineering Sciences* 365.1851 (2007): 303-315.

Fujita, Masanori, and Mamoru Iwata. "Reuse system of building steel structures." *Structure and Infrastructure Engineering* 4.3 (2008): 207-220.

Gorgolewski, Mark, Vera Straka, Jordan Edmonds, and Carmela Sergio. *Facilitating Greater Reuse and Recycling of Structural Steel in the Construction and Demolition Process*. Rep. Ryerson University. Canadian Institute of Steel Construction, 20 Mar. 2006. Web. 3 Feb. 2015.

Gorgolewski, Mark. "Designing with reused building components: some challenges." *Building Research & Information* 36.2 (2008): 175-188.

Gorgolewski, Mark. "The implications of reuse and recycling for the design of steel buildings." *Canadian Journal of Civil Engineering* 33.4 (2006): 489-496.

Hoult, N. A., P. R. A. Fidler, P. J. Bennett, C. R. Middleton, S. Pottle, K. Duguid, G. Bessant, R. McKoy, and K. Soga. "Large-scale WSN installation for pervasive monitoring of civil infrastructure in London." *Structural Health Monitoring, Naples, Italy* (2010): 214-219.

Li, D. S., L. Ren, H. N. Li, and G. B. Song, "Structural Health Monitoring of a Tall Building during Construction with Fiber Bragg Grating Sensors," International Journal of Distributed Sensor Networks, vol. 2012, Article ID 272190, 10 pages, 2012. doi:10.1155/2012/272190

LORD MicroStrain. "Wireless Networks." *LORD MicroStrain Sensing Networks*. LORD MicroStrain, n.d. Web. 17 Mar. 2015.

Lynch, Jerome P., and Kenneth J. Loh. "A summary review of wireless sensors and sensor networks for structural health monitoring." Shock and Vibration Digest 38.2 (2006): 91-130.

Mcconnell, Jennifer, Thomas Schumacher, Erik T. Thostenson, Tayler Wennick, and Philipp Keller. "Evaluating Structural Steel for Reuse through Field Monitoring." Proc. of 37th IABSE Symposium on Engineering for Progress, Nature and People, Spain, Madrid. International Association for Bridge and Structural Engineering (IABSE), 2014.

McCormac, Jack C., and Stephen F. Csernak. *Structural Steel Design*. 5th ed. Boston: Prentice Hall, 2012. Print.

Ni, Y. Q., Y. Xia, W.Y. Liao, and J.M. Ko. "Technology innovation in developing the structural health monitoring system for Guangzhou New TV Tower." *Structural Control and Health Monitoring* 16.1 (2009): 73-98.

Nordblom, Todd, and Jacob Galbreath. "Wireless Sensor Networks for Improved Long-Term Bridge Performance." LORD MicroStrain Sensing Systems. MicroStrain, Inc., 2012. Web. 11 June 2014.

Nunez, T. R., R. L. Boroschek, and A. Larrain. "Validation of a construction process using a structural health monitoring network." Journal of Performance of Constructed Facilities 27.3 (2011): 270-282.

Pulaski, Michael, Bradley Guy, Christopher Hewitt, and Michael Horman. "Design for deconstruction: Material reuse and constructability." *The Pittsburgh Papers: Best of Greenbuild 2003* (2003): 74-81.

Rainieri, C., and G. Fabbrocino. "Experiences of Structural Health Monitoring in Operational Conditions." *Fifth European Workshop on Structural Health Monitoring 2010*. DEStech Publications, Inc, 2010.

Sarja, Asko. *Integrated Life Cycle Design of Structures*. London: Spon, 2002. Print.

Scott, David W. "The L_2 Theory of Univariate Histograms." *Multivariate Density Estimation: Theory, Practice, and Visualization*. New York: Wiley, 1992. N. pag. Print.

Silverstein, Scott Aaron. *Applying" Design for Disassembly" to Connection Design in Steel Structures*. Diss. Massachusetts Institute of Technology, 2009.

Webster, Marc D., and Daniel T. Costello. "Designing structural systems for deconstruction: how to extend a new building's useful life and prevent it from

going to waste when the end finally comes." *Proceedings of the 2005 Greenbuild Conference, Atlanta, USA*. 2005.

Weisenberger, Geoff. "The Fabrication Factor." *Modern Steel Construction* 50.7 (2010): 56-57.

World Steel Association. "World Steel in Figures 2013." *World Steel Association*. World Steel Association, 2013. Web. 16 Mar. 2015.

Yellishetty, Mohan, Gavin Mudd, P.G. Ranjith, and A. Tharumarajah. "Environmental life-cycle comparisons of steel production and recycling: sustainability issues, problems and prospects." *Environmental Science & Policy* 14.6 (2011): 650-663.

Appendix A

PURNELL HALL INSTRUMENTATION

The following Figures 28 through 32 show the gauge and node locations for the WSN utilized in Purnell Hall. All members were instrumented at RCF prior to delivery at the University of Delaware. Reference Figure 12 for member locations in Purnell Hall.

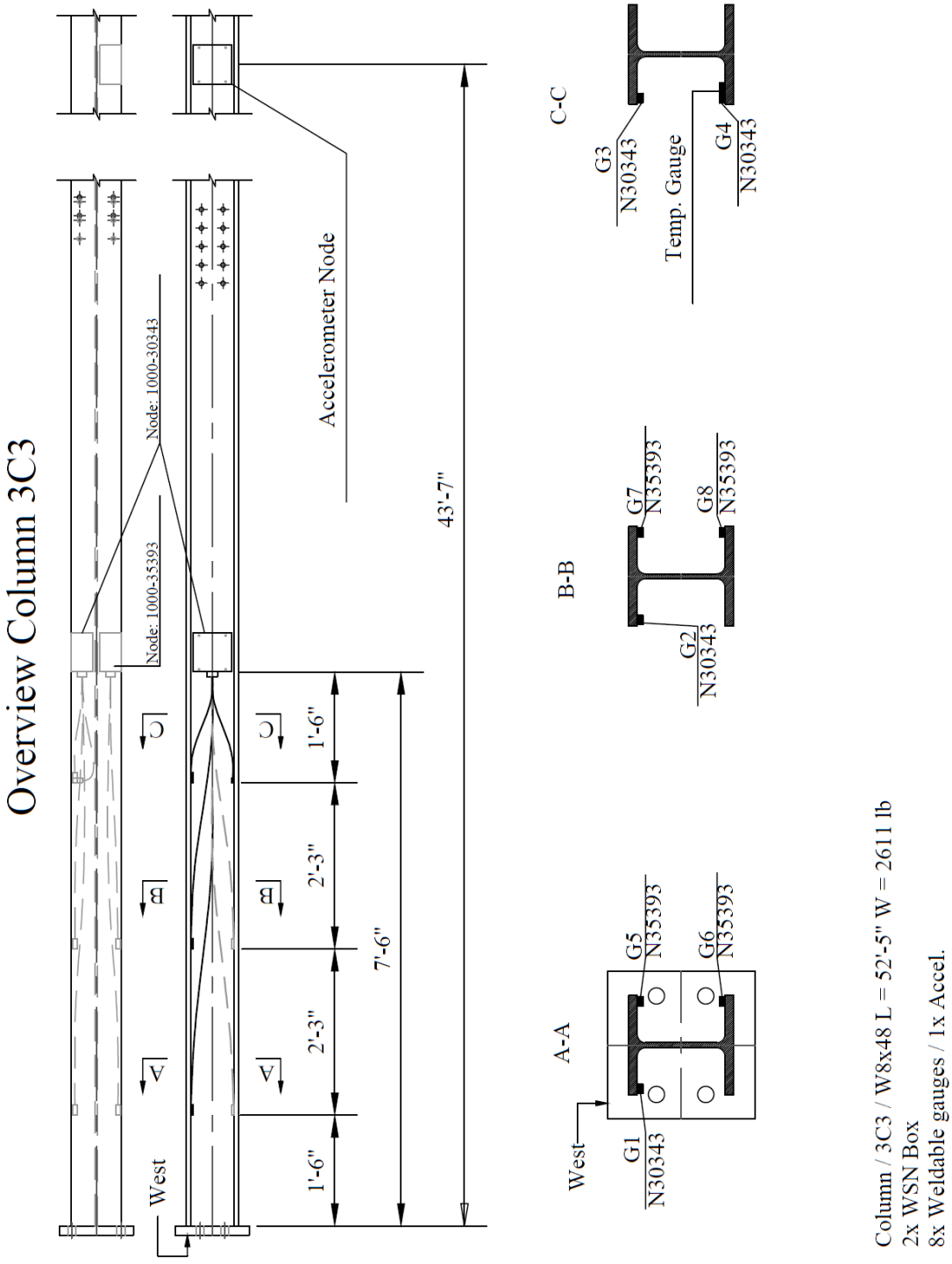

Figure 28: Instrumentation of Purnell Hall Column 3C3 (Adapted from Philipp Keller)

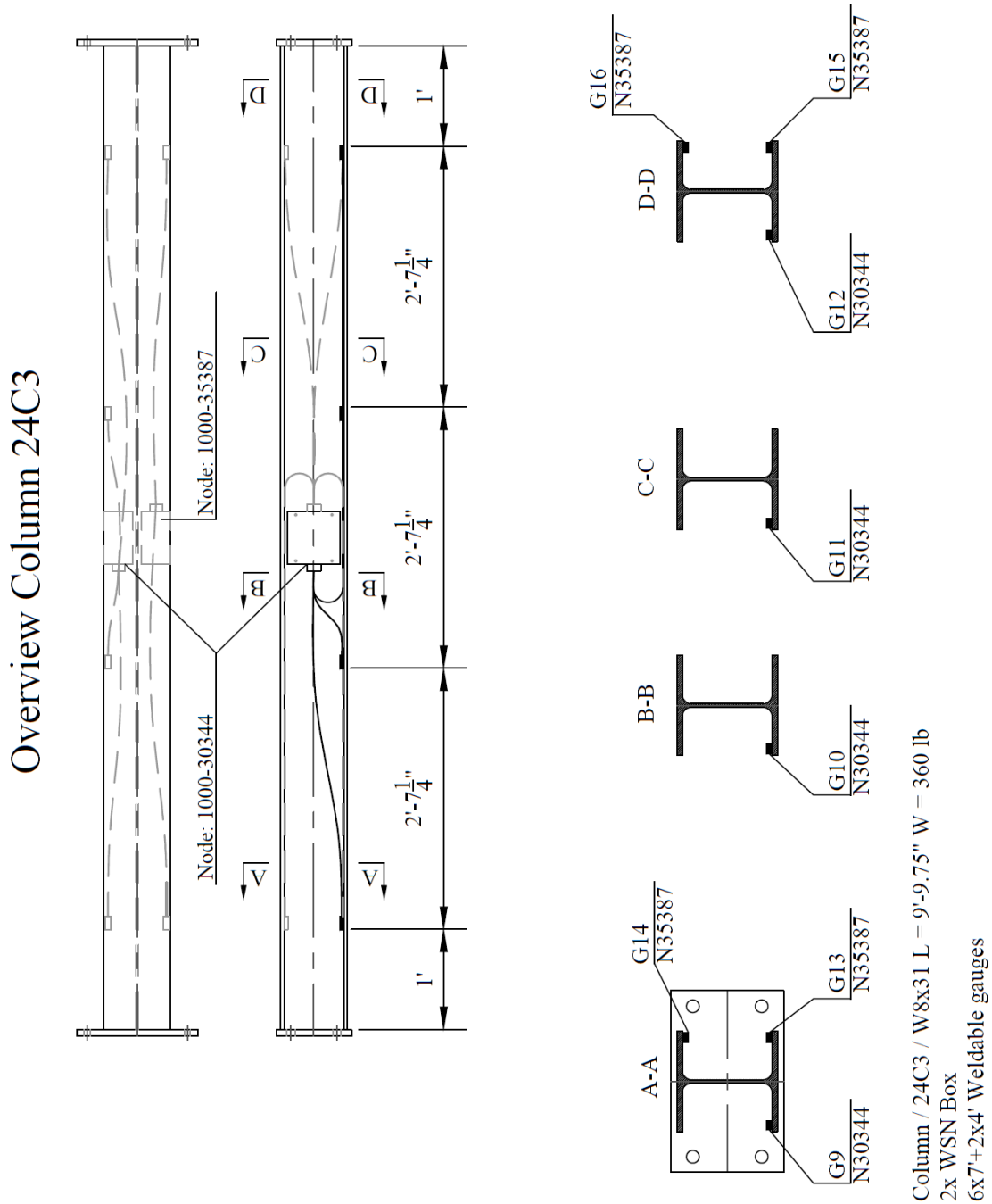

Figure 29: Instrumentation of Purnell Hall Column 24C3 (Adapted from Philipp Keller)

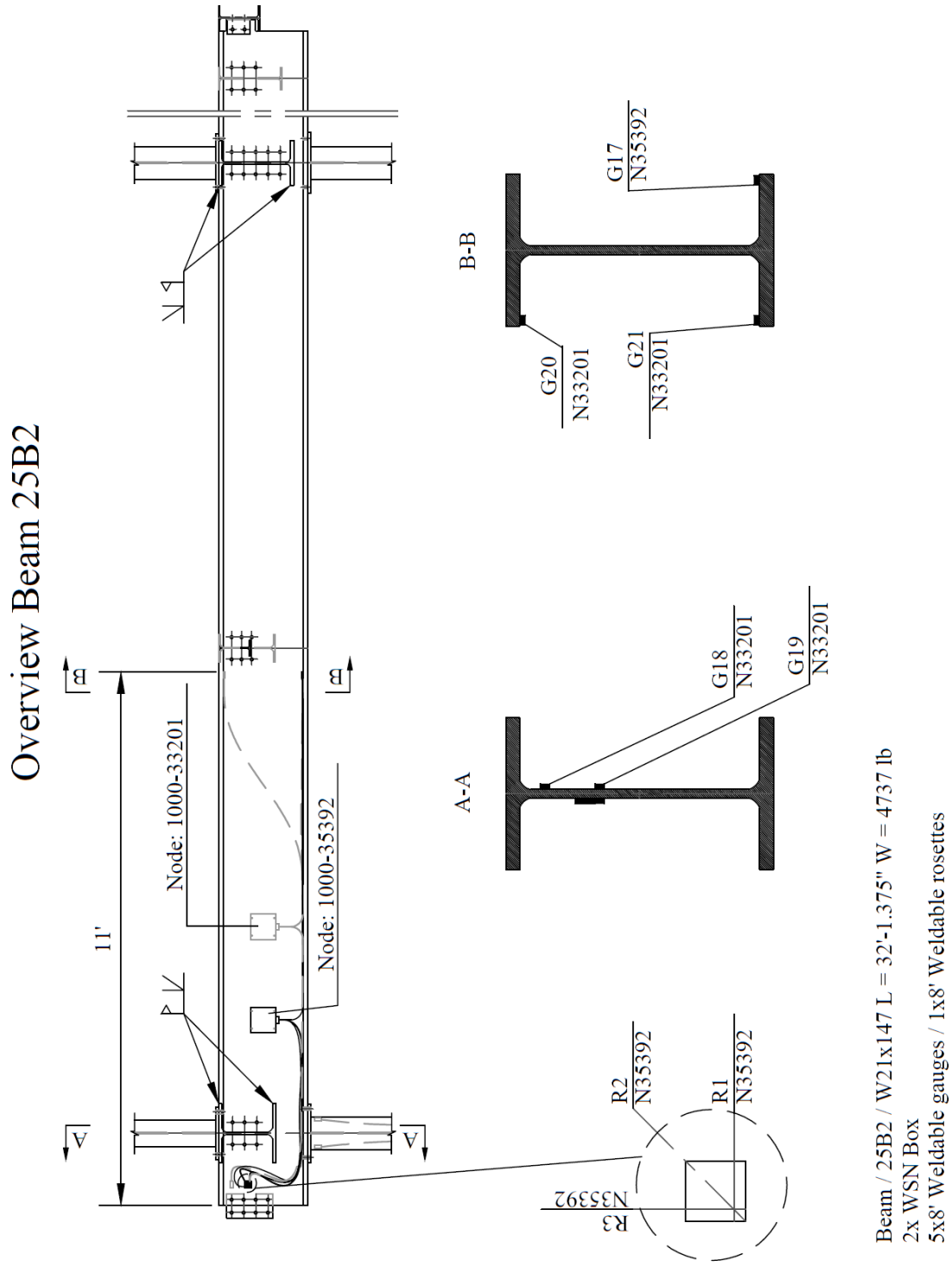

Figure 30: Instrumentation of Purnell Hall Beam 25B2 (Adapted from Philipp Keller)

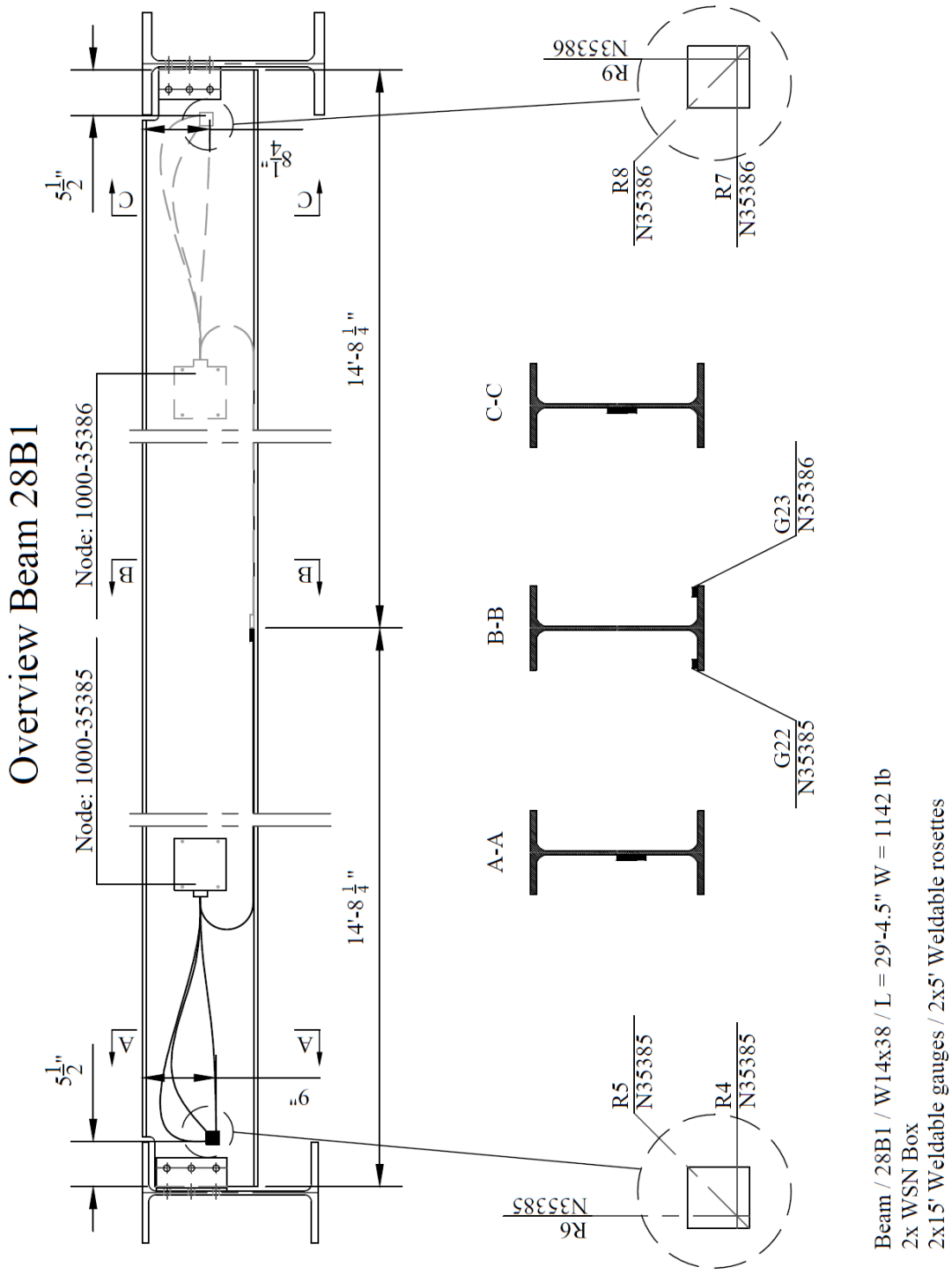

Figure 31: Instrumentation of Purnell Hall Beam 28B1 (Adapted from Philipp Keller)

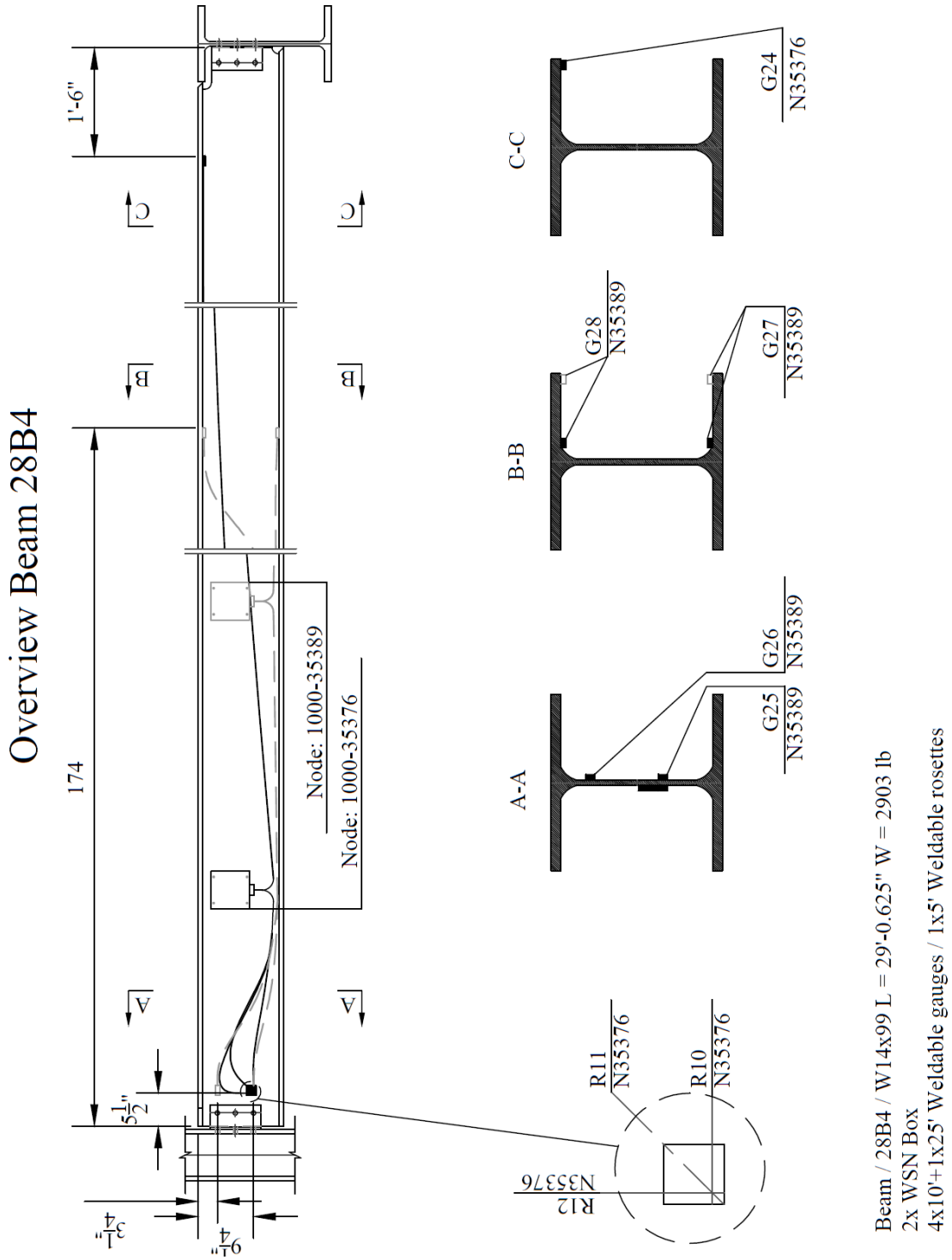

Figure 32: Instrumentation of Purnell Hall Beam 28B4 (Adapted from Philipp Keller)

Appendix B

ENTIRE DATA COLLECTION FOR ALL GAUGE SETS ON PURNELL HALL

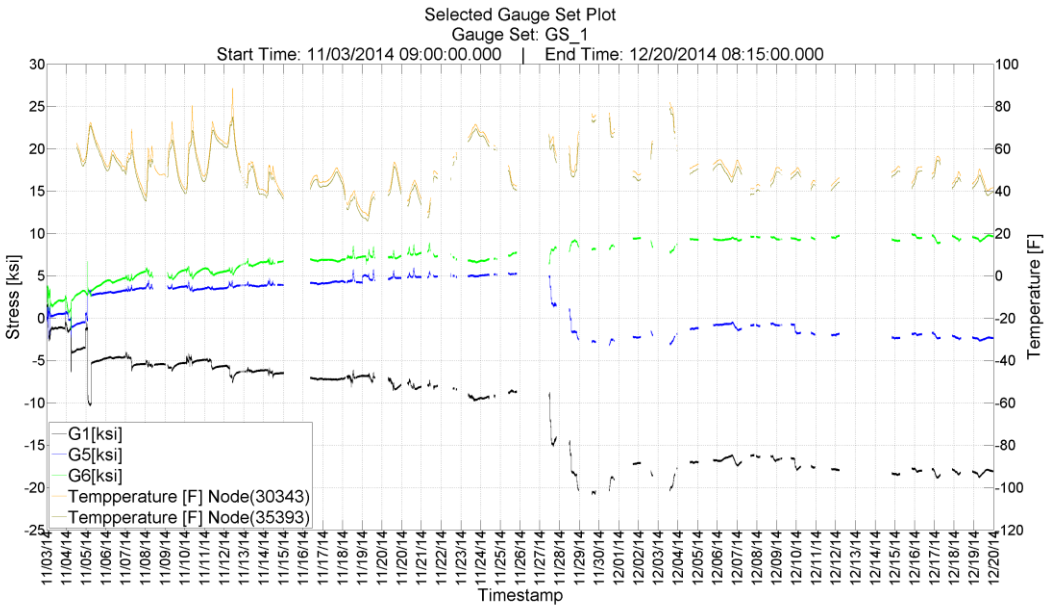

Figure 33: Data Collection for Gauge Set 1

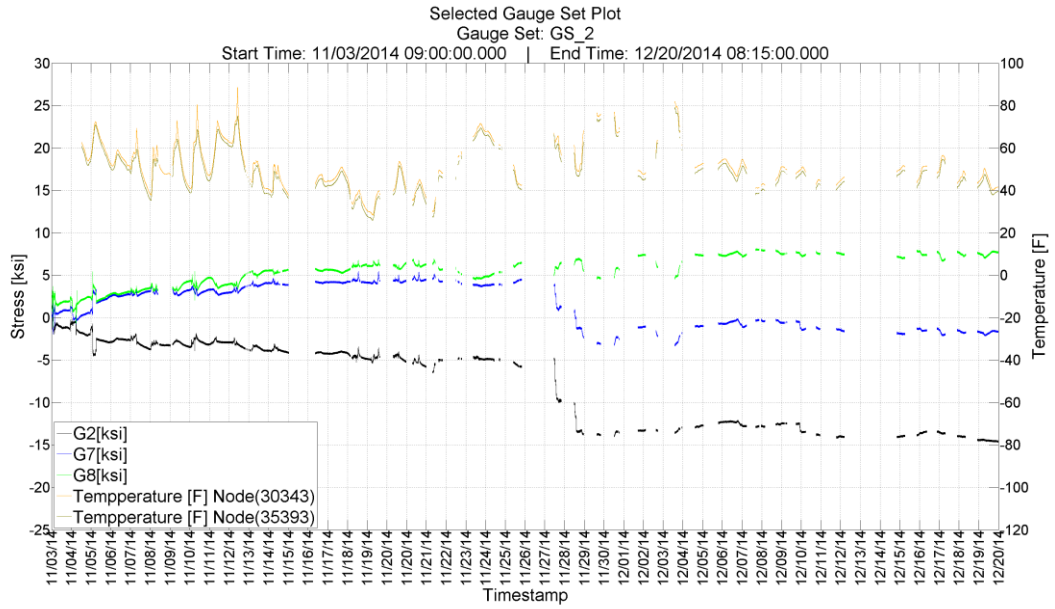

Figure 34: Data Collection for Gauge Set 2

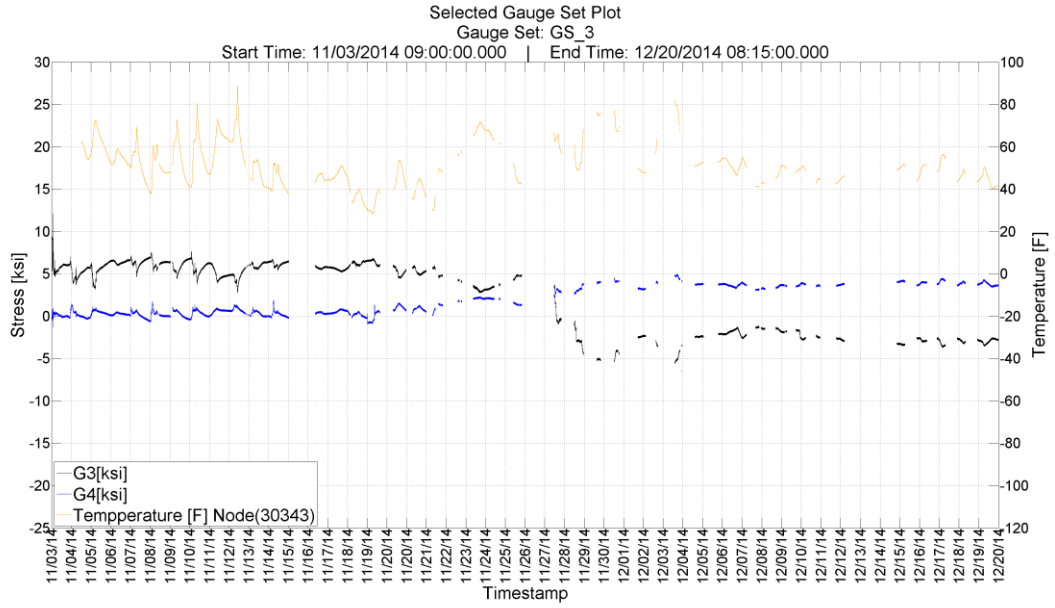

Figure 35: Data Collection for Gauge Set 3

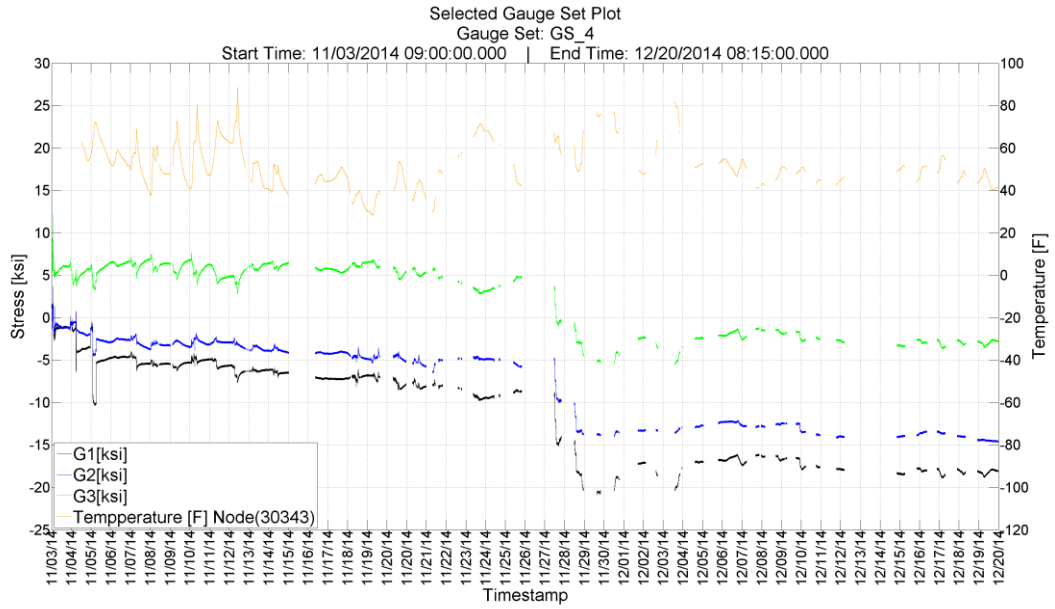

Figure 36: Data Collection for Gauge Set 4

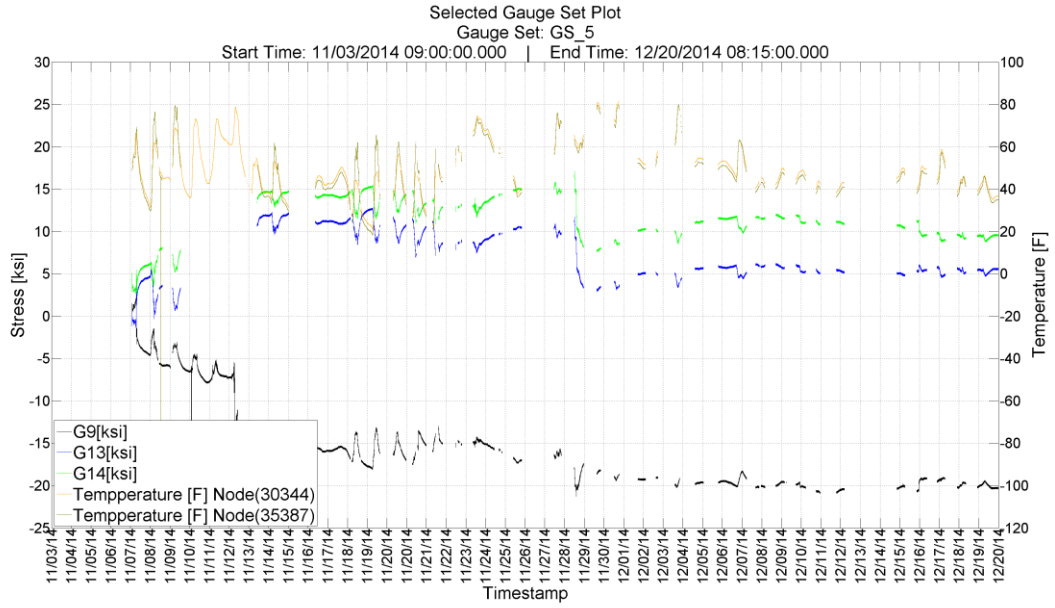

Figure 37: Data Collection for Gauge Set 5

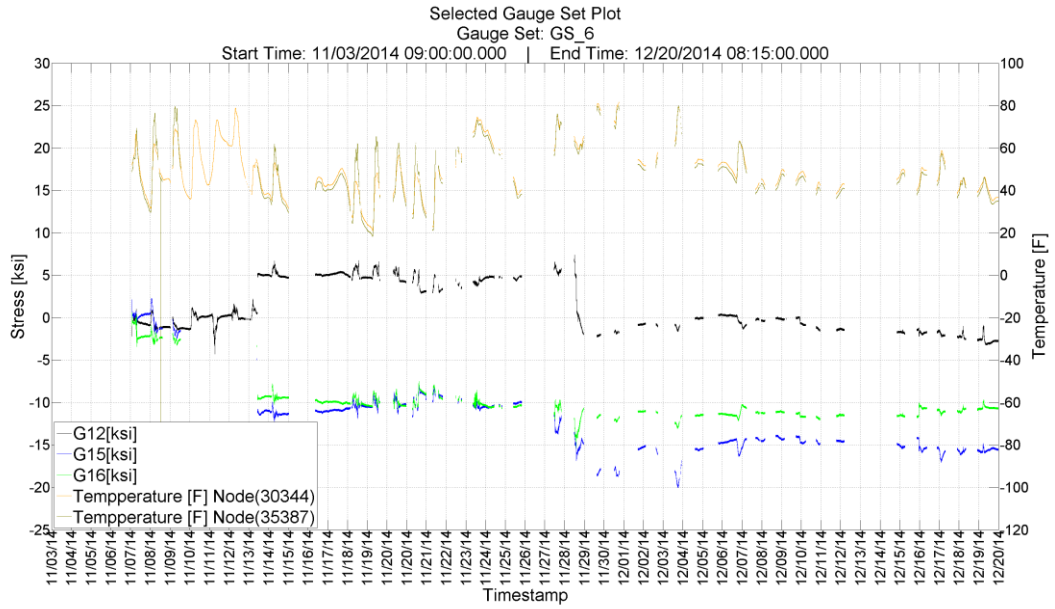

Figure 38: Data Collection for Gauge Set 6

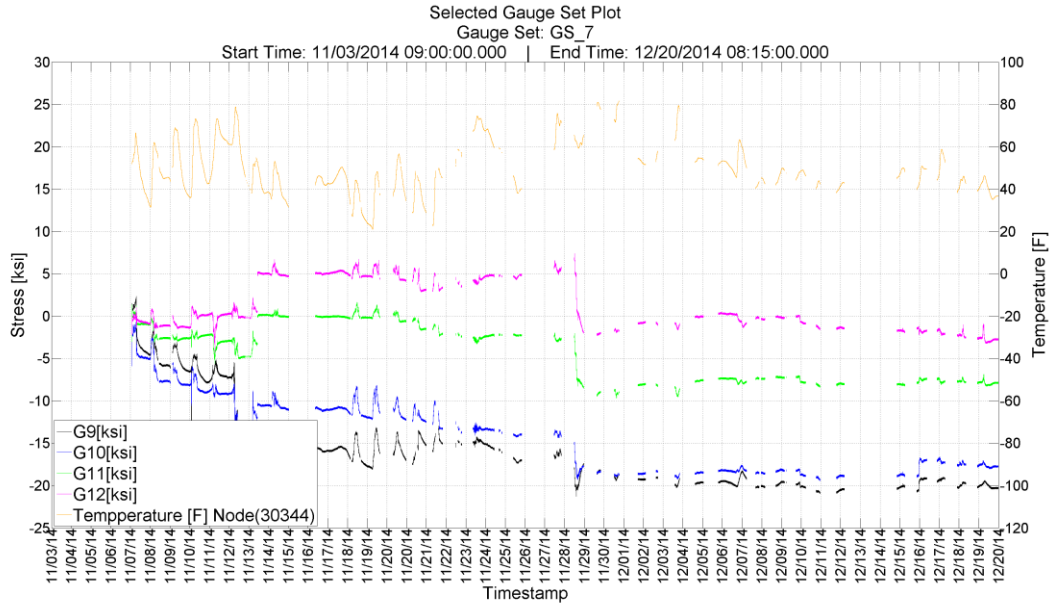

Figure 39: Data Collection for Gauge Set 7

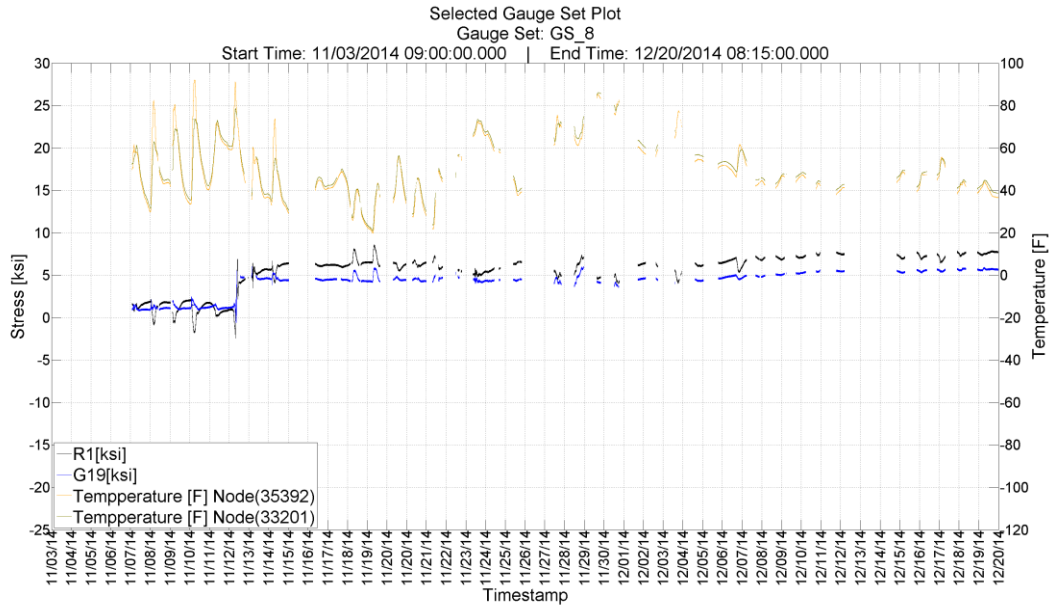

Figure 40: Data Collection for Gauge Set 8

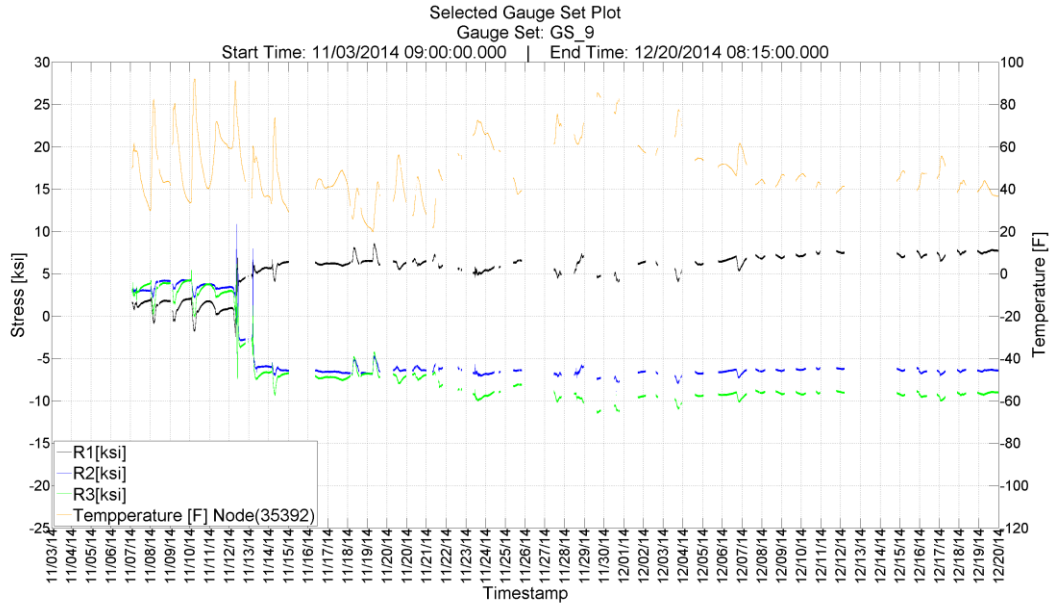

Figure 41: Data Collection for Gauge Set 9

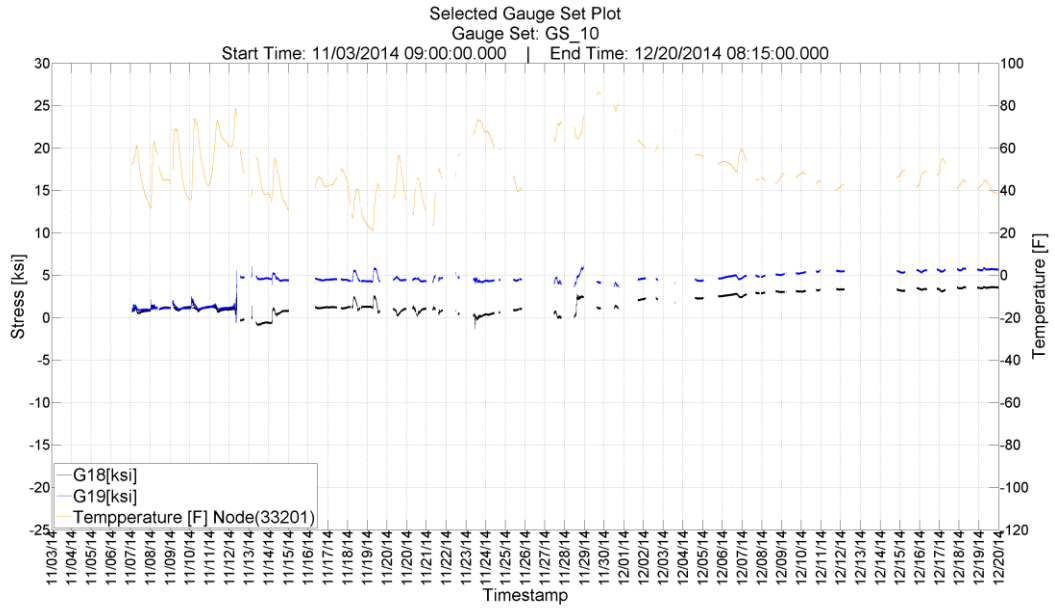

Figure 42: Data Collection for Gauge Set 10

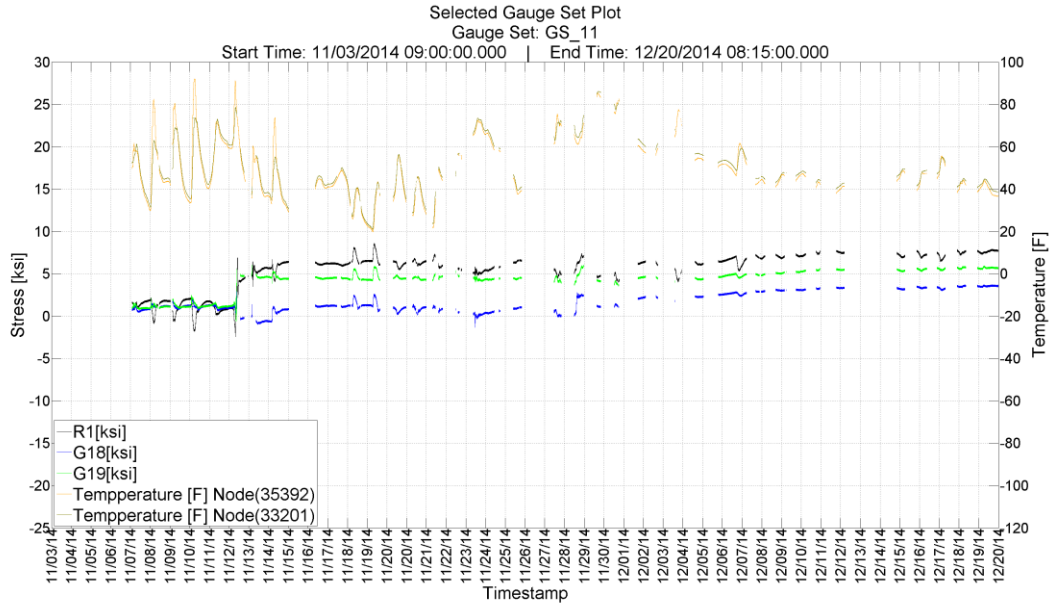

Figure 43: Data Collection for Gauge Set 11

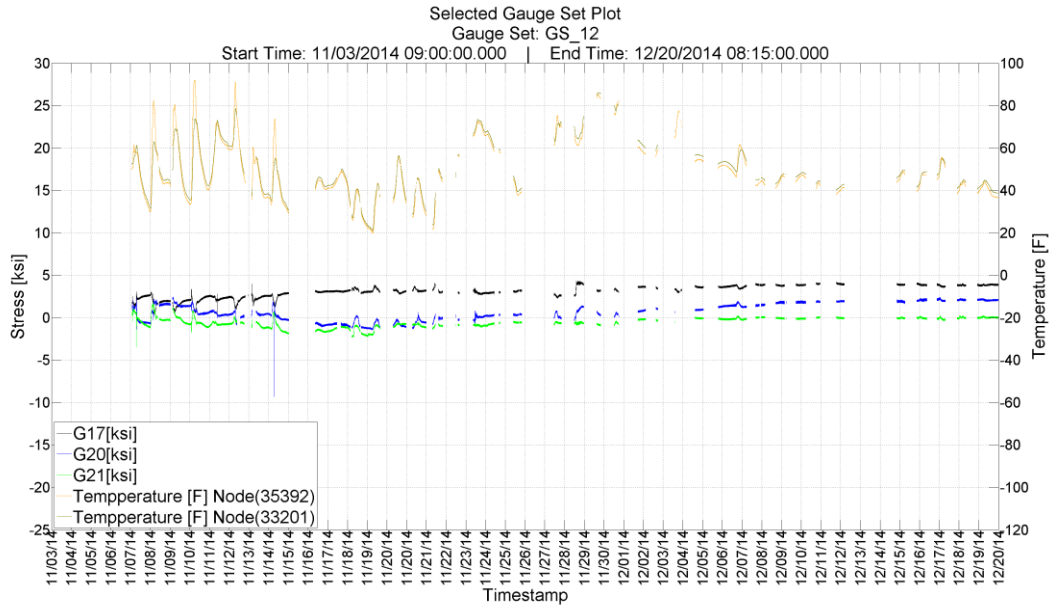

Figure 44: Data Collection for Gauge Set 12

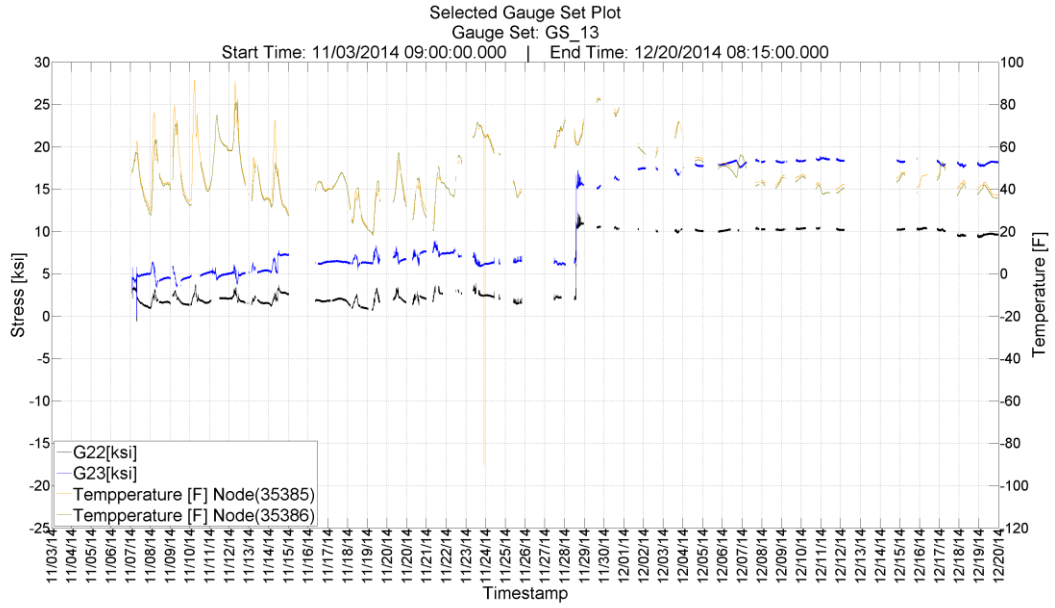

Figure 45: Data Collection for Gauge Set 13

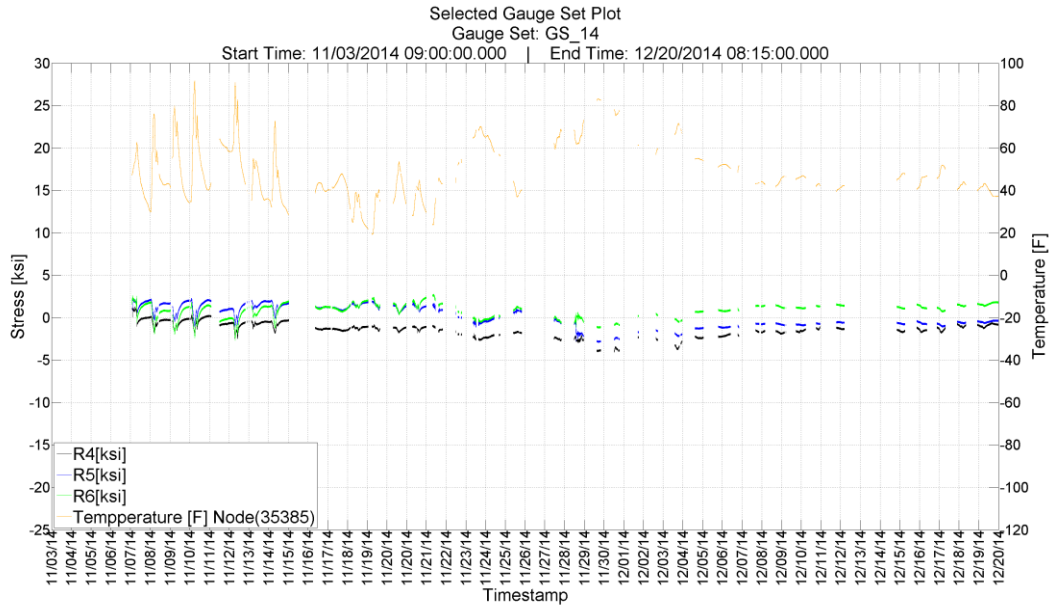

Figure 46: Data Collection for Gauge Set 14

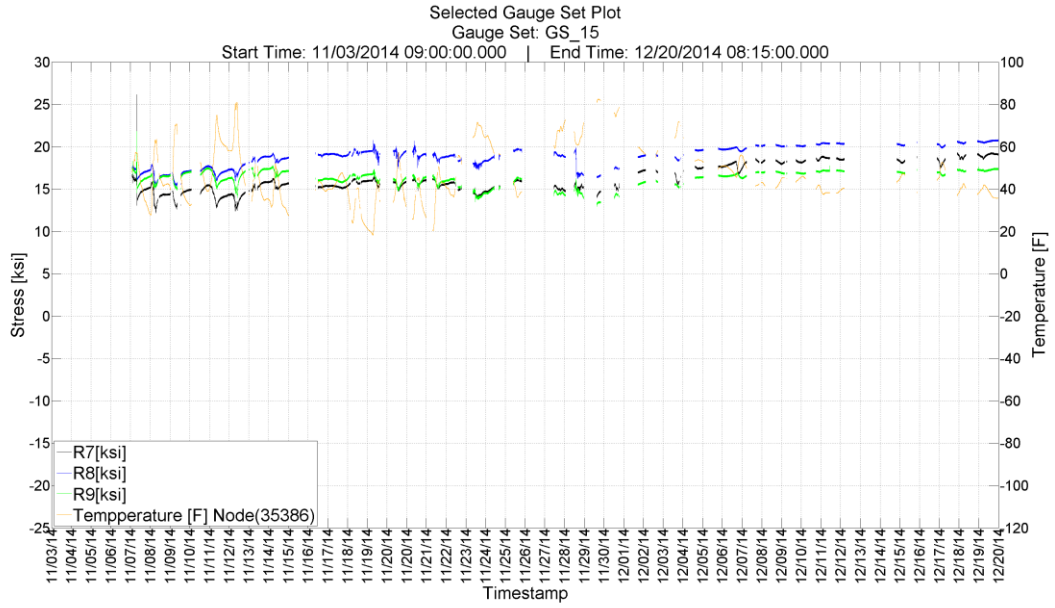

Figure 47: Data Collection for Gauge Set 15

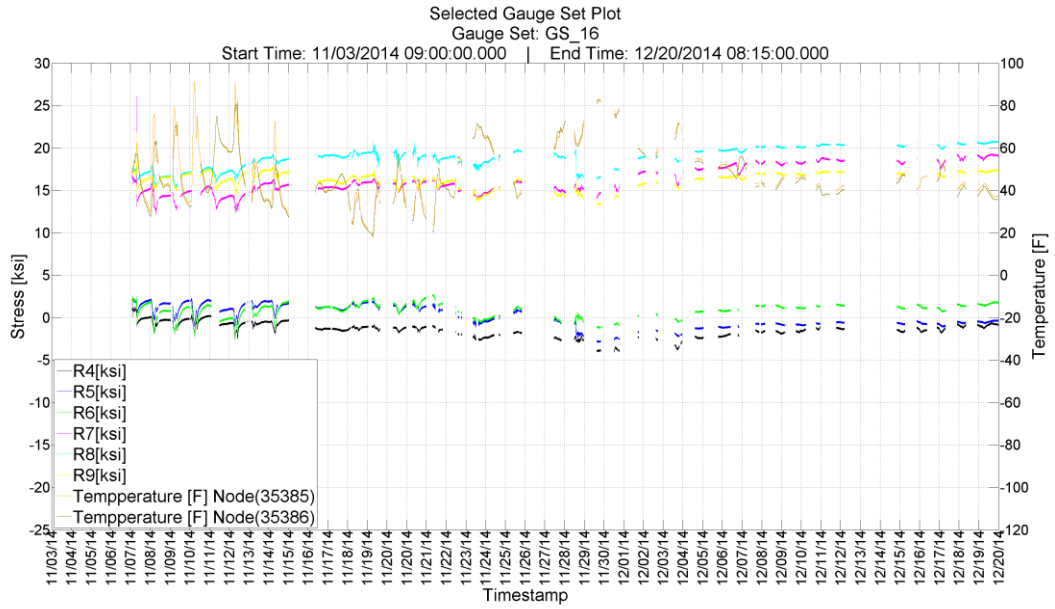

Figure 48: Data Collection for Gauge Set 16

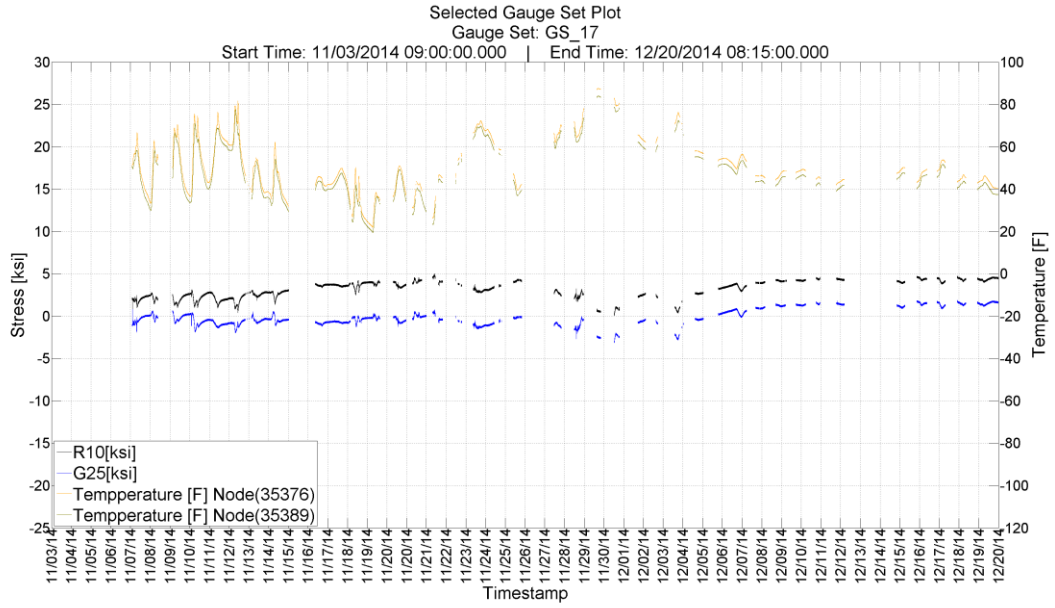

Figure 49: Data Collection for Gauge Set 17

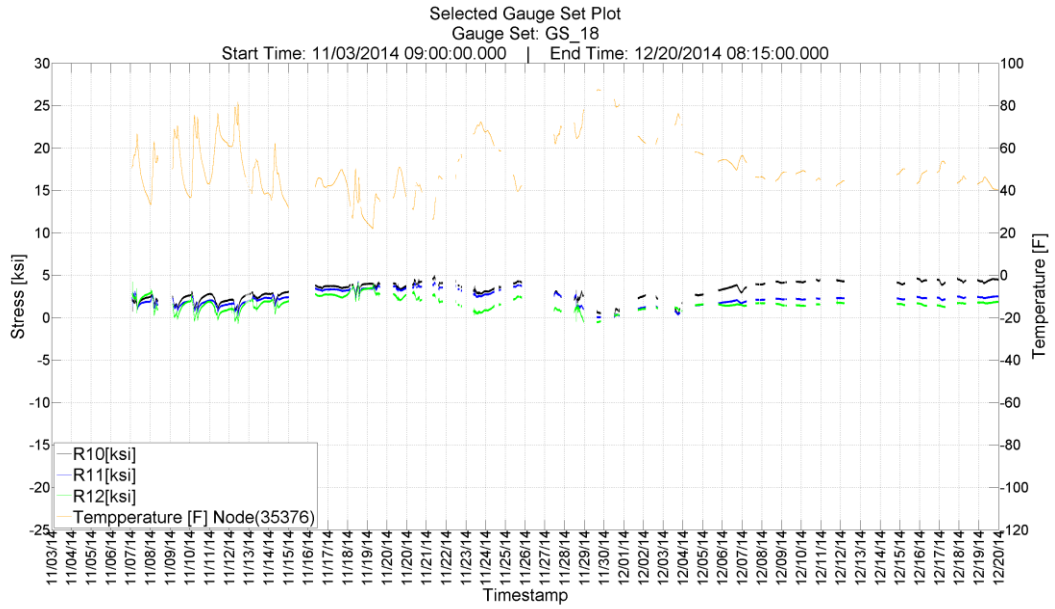

Figure 50: Data Collection for Gauge Set 18

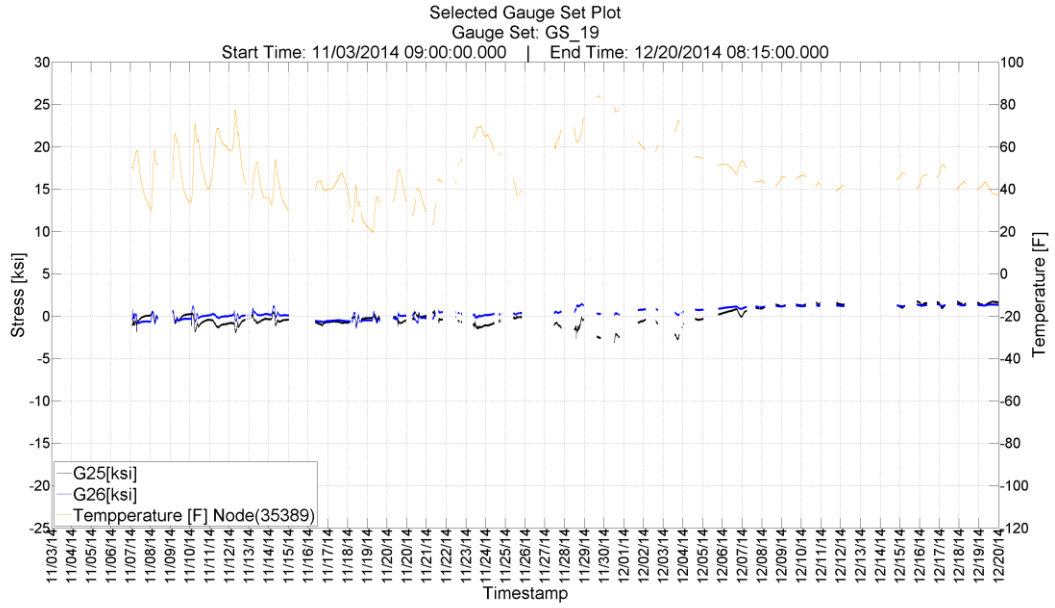

Figure 51: Data Collection for Gauge Set 19

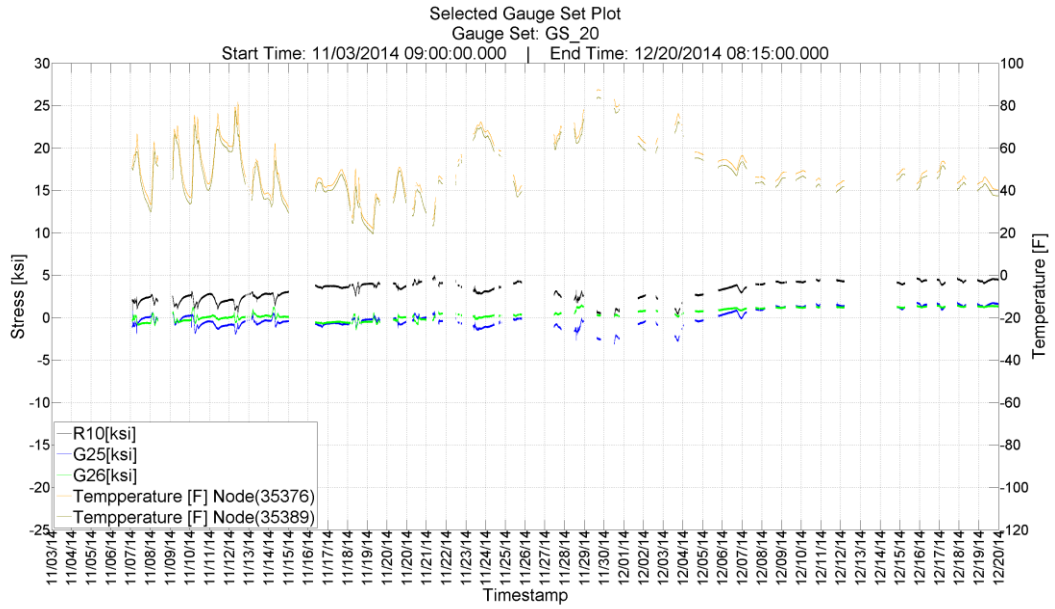

Figure 52: Data Collection for Gauge Set 20

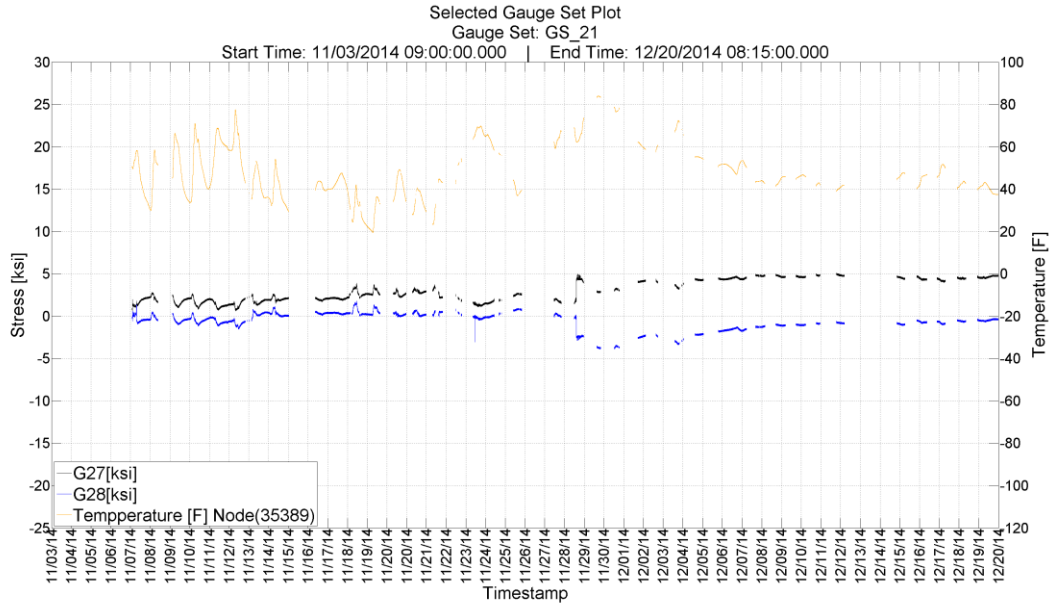

Figure 53: Data Collection for Gauge Set 21

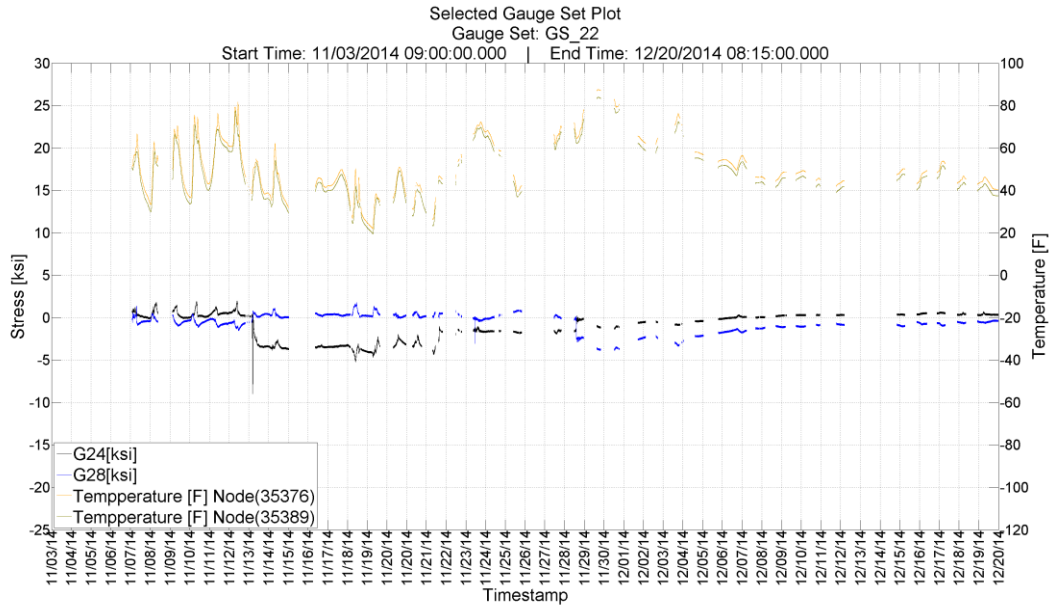

Figure 54: Data Collection for Gauge Set 22

Appendix C

GAUGE SET'S MAXIMUM POSITIVE AND NEGATIVE STRESSES

Table 9: Every gauge set's maximum positive stress and all gauge stresses at that time.

POSITIVE MAXIMUM STRESSES			
SET NUMBER	**DATE/TIME**	**GAUGES IN SET**	**MAX POSITIVE STRESS**
1	12/16/2014 07:07:37.012	G1	-17.6774
		G5	-1.7604
		G6	**10.0207**
1	12/16/2014 07:07:37.637	G1	-17.7083
		G5	-1.7886
		G6	**10.0207**
2	12/08/2014 07:15:04.449	G2	-12.8902
		G7	-0.2823
		G8	**8.1435**
2	12/08/2014 07:15:04.887	G2	-12.8902
		G7	-0.2823
		G8	**8.1435**
3	11/03/2014 10:40:21.699	**G3**	**12.1405**
		G4	-1.1991
4	11/03/2014 10:40:21.699	G1	2.3126
		G2	3.6345
		G3	**12.1405**
5	11/29/2014 07:46:04.449	G9	-18.1524
		G13	11.6568
		G14	**17.1381**
6	11/29/2014 07:45:36.199	**G12**	**7.3777**
		G15	-13.6081
		G16	-12.0666
7	11/29/2014 07:45:36.199	G9	-18.0991
		G10	-14.9324
		G11	-2.1108
		G12	**7.3777**
		G28	-1.1458

Table 9: Continued

8	11/19/2014 09:08:21.949	**R1**	**8.5916**
		G19	5.7850
9	11/12/2014 13:06:41.887	R1	0.2408
		R2	**10.8712**
		R3	6.0510
10	11/29/2014 18:22:13.387	G18	2.4558
		G19	**6.0274**
10	11/29/2014 18:22:34.012	G18	2.4699
		G19	**6.0274**
11	11/19/2014 09:08:21.949	**R1**	**8.5916**
		G18	2.4727
		G19	5.7850
12	11/29/2014 09:46:54.824	**G17**	**4.3588**
		G20	0.6129
		G21	-0.5238
13	12/11/2014 11:54:35.012	G22	10.4414
		G23	**18.8928**
13	12/11/2014 12:07:10.012	G22	10.4414
		G23	**18.8928**
13	12/11/2014 18:20:09.012	G22	10.4414
		G23	**18.8928**
13	12/11/2014 18:40:46.012	G22	10.4414
		G23	**18.8928**
14	11/22/2014 07:50:19.199	R4	-1.0759
		R5	1.4251
		R6	**2.8060**
15	11/07/2014 14:32:28.699	**R7**	**26.1682**
		R8	20.7336
		R9	21.6546
15	11/07/2014 14:32:28.824	**R7**	**26.1682**
		R8	20.7616
		R9	21.6321
16	11/07/2014 14:32:28.699	R4	0.7124
		R5	1.2704
		R6	1.3149
		R7	**26.1682**
		R8	20.7336
		R9	21.6546

Table 9: Continued

16	11/07/2014 14:32:28.824	R4	0.6899
		R5	1.2591
		R6	1.2670
		R7	**26.1682**
		R8	20.7616
		R9	21.6321
17	11/22/2014 08:48:27.137	**R10**	**4.9942**
		G25	0.3580
18	11/22/2014 08:48:27.137	**R10**	**4.9942**
		R11	4.0872
		R12	2.7112
19	12/18/2014 07:09:41.074	**G25**	**1.8692**
		G26	1.5082
20	11/22/2014 08:48:27.137	**R10**	**4.9942**
		G25	0.3580
		G26	-0.0373
21	12/12/2014 07:37:51.762	**G27**	**5.0941**
		G28	-0.7509
22	11/12/2014 13:34:59.449	**G24**	**1.9745**
		G28	-1.1458

Table 10: Every gauge set's maximum negative stress and all gauge stresses at that time.

NEGATIVE MAXIMUM STRESSES			
SET NUMBER	**DATE/TIME**	**GAUGES IN SET**	**MAX NEGATIVE STRESS**
1	11/30/2014 14:30:34.324	**G1**	**-20.8529**
		G5	-2.8549
		G6	8.1735
2	12/19/2014 13:05:19.449	**G2**	**-14.6883**
		G7	-1.7535
		G8	7.3571
3	12/04/2014 15:30:49.387	**G3**	**-6.4791**
		G4	4.1701
4	11/30/2014 14:30:34.324	**G1**	**-20.8529**
		G2	-13.8551
		G3	-5.1203
		G28	0.6902

Table 10: Continued

5	11/29/2014 07:24:38.324	**G9**	**-21.2698**
		G13	11.1981
		G14	16.5755
6	12/04/2014 15:31:19.137	G12	-0.9383
		G15	**-20.0495**
		G16	-11.5099
7	11/29/2014 07:24:38.324	**G9**	**-21.2698**
		G10	-15.0029
		G11	-2.4317
		G12	6.7623
8	11/12/2014 14:18:58.512	**R1**	**-2.4256**
		G19	5.4806
9	11/30/2014 14:28:47.637	R1	4.7832
		R2	-7.2935
		R3	**-11.5042**
10	11/24/2014 08:35:58.512	**G18**	**-1.3329**
		G19	4.5843
11	11/12/2014 14:18:58.512	**R1**	**-2.4256**
		G18	2.7122
		G19	5.4806
12	11/14/2014 09:12:21.637	G17	1.9989
		G20	**-9.2988**
		G21	0.5797
13	11/07/2014 09:16:37.949	**G22**	**-0.6863**
		G23	3.9733
14	12/01/2014 08:23:50.762	**R4**	**-4.0705**
		R5	-2.4012
		R6	-0.7483
15	11/08/2014 08:18:34.074	**R7**	**-12.1641**
		R8	17.8873
		R9	16.7831
16	12/01/2014 08:23:50.762	**R4**	**-4.0705**
		R5	-2.4012
		R6	-0.7483
		R7	15.5075
		R8	17.5928
		R9	14.3052
17	12/01/2014 08:51:19.262	R10	1.0652
		G25	**-3.1218**
18	11/12/2014 08:02:07.199	**R10**	**-0.6985**
		R11	1.7372
		R12	1.4350

Table 10: Continued

19	12/01/2014 08:51:19.262	**G25**	**-3.1218**
		G26	0.3766
20	12/01/2014 08:51:19.262	R10	1.0652
		G25	**-3.1218**
		G26	0.3766
21	11/30/2014 10:13:05.074	G27	2.9509
		G28	**-3.8673**
22	11/13/2014 08:59:43.512	**G24**	**-8.9752**
		G28	0.7241
22	11/13/2014 09:00:05.699	**G24**	**-8.9752**
		G28	0.6620
22	11/13/2014 09:00:09.012	**G24**	**-8.9752**

Appendix D

STEEL SHOP DRAWINGS SUBMITTED TO THE SUMMIT STEEL, INC.

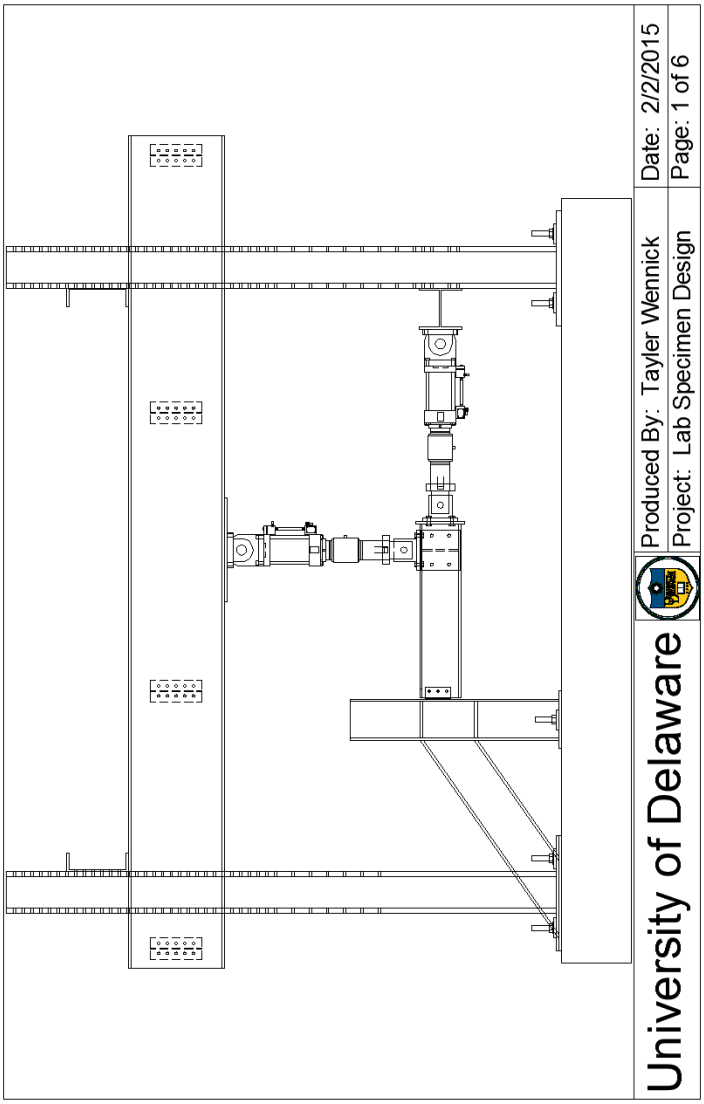

Figure 55: Steel Shop Drawing, page 1 of 6, submitted to Summit Steel, Inc. for fabrication

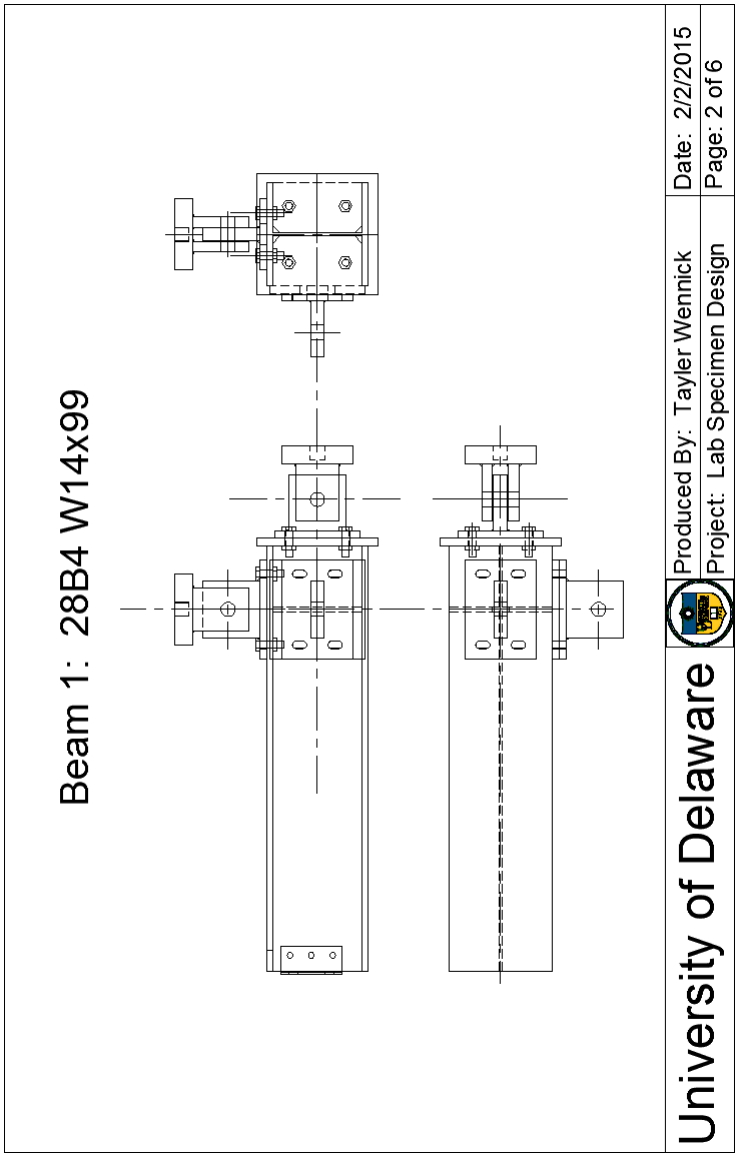

Figure 56: Steel Shop Drawing, page 2 of 6, submitted to Summit Steel, Inc. for fabrication

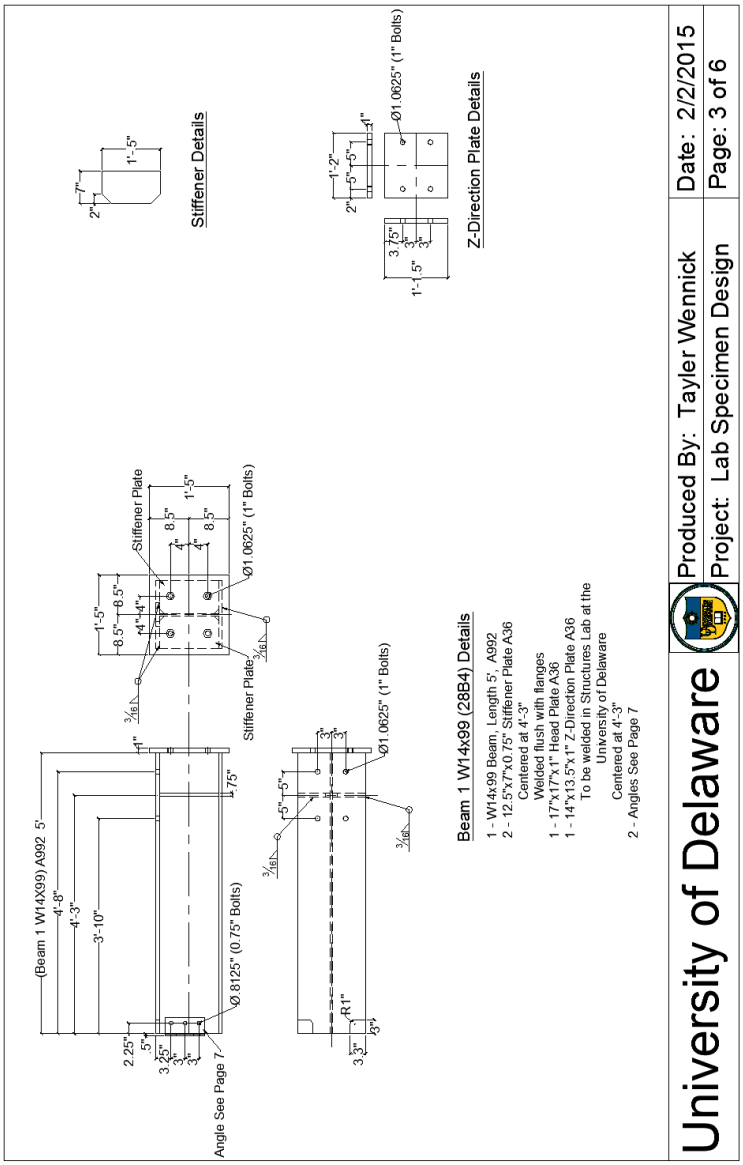

Figure 57: Steel Shop Drawing, page 3 of 6, submitted to Summit Steel, Inc. for fabrication

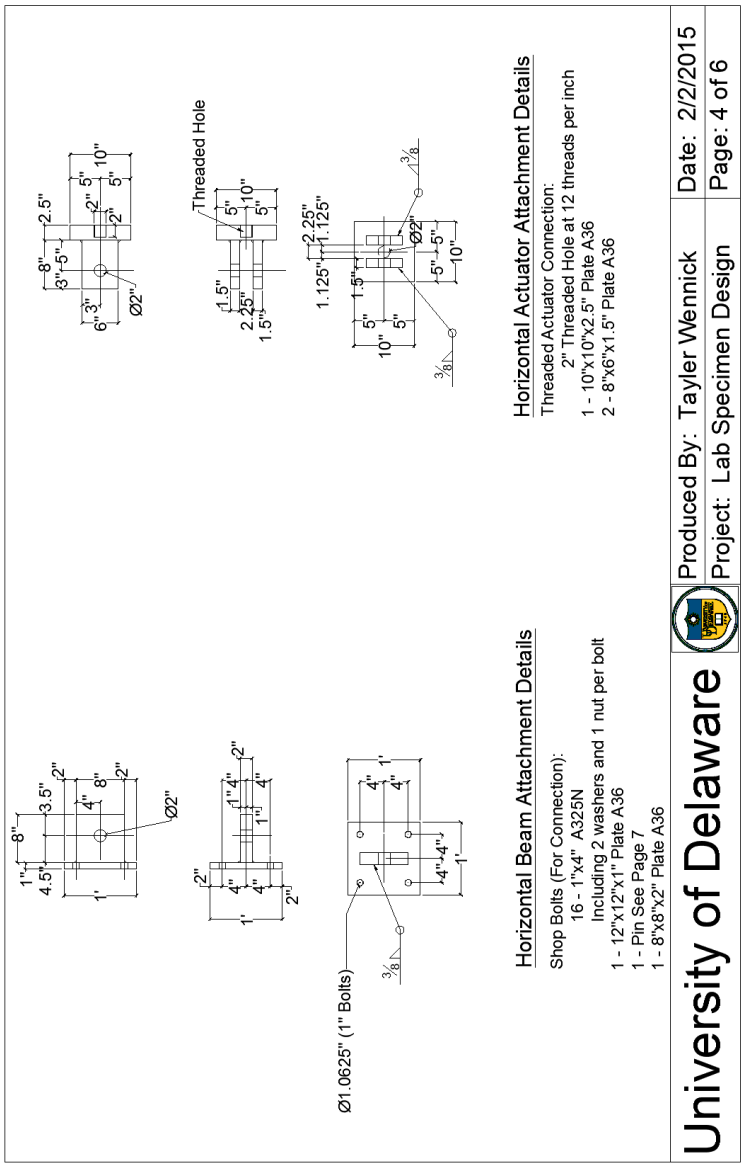

Figure 58: Steel Shop Drawing, page 4 of 6, submitted to Summit Steel, Inc. for fabrication

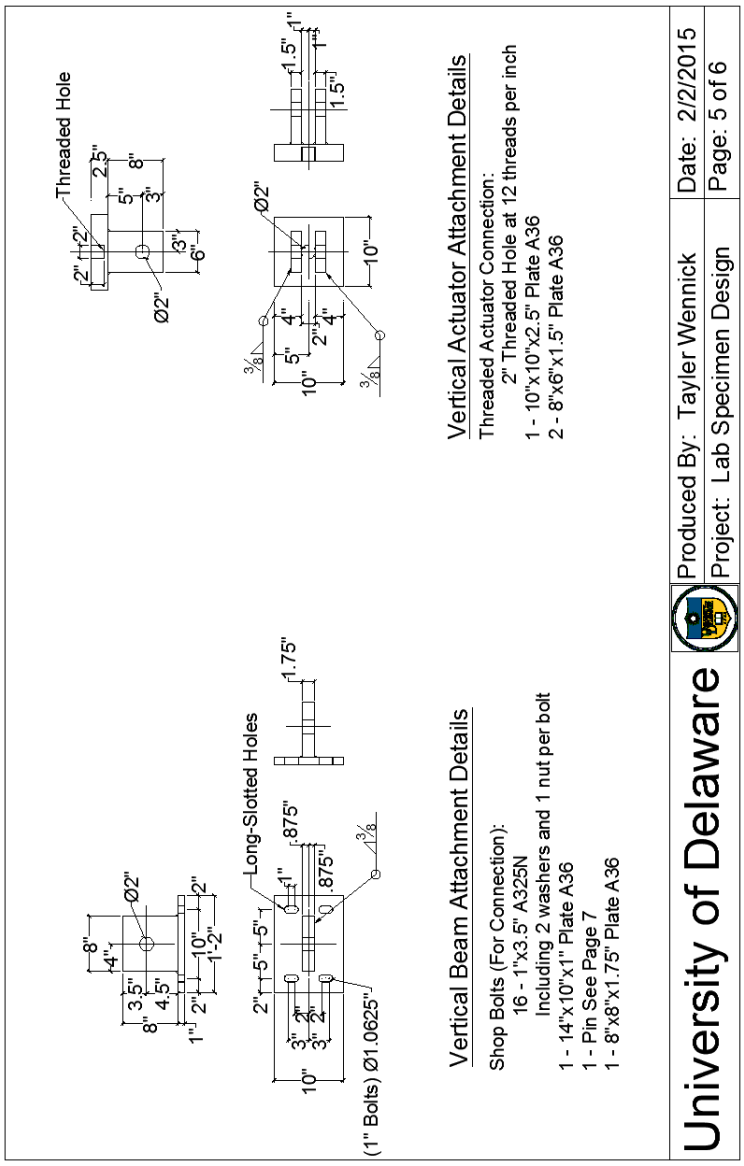

Figure 59: Steel Shop Drawing, page 5 of 6, submitted to Summit Steel, Inc. for fabrication

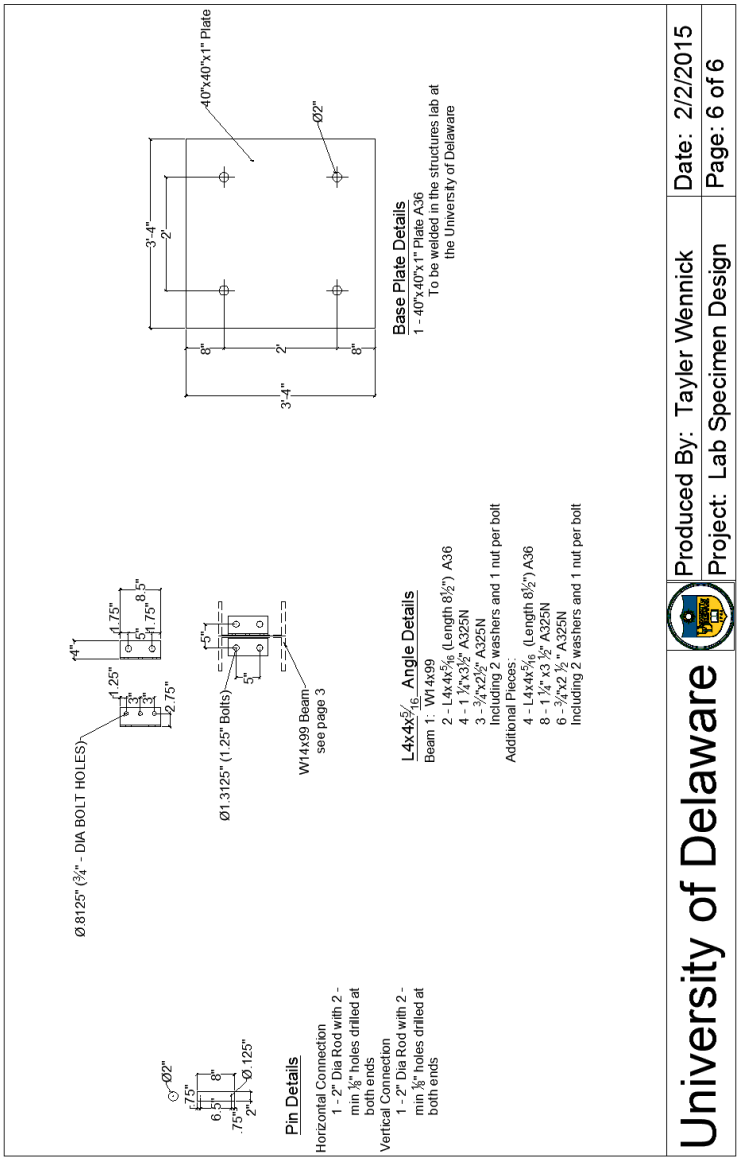

Figure 60: Steel Shop Drawing, page 6 of 6, submitted to Summit Steel, Inc. for fabrication